A single coelomic cell type is involved in both immune and respiratory functions of the coastal bioindicator annelid: Capitella C-Channel1 from the English Channel

Céline Boidin-Wichlacz, Ann C. Andersen, Nathalie Jouy, Stephane Hourdez, Aurélie Tasiemski

A single coelomic cell type is involved in both immune and respiratory functions of the coastal bioindicator annelid: *Capitella* C-Channel1 from the English Channel

Céline Boidin-Wichlacz[a]*, *Ann C. Andersen*[b], *Nathalie Jouy*[d], *Stéphane Hourdez*[c], *Aurélie Tasiemski*[a]

[a] Univ. Lille, CNRS, Inserm, CHU Lille, Institut Pasteur de Lille, U1019 - UMR 9017 - CIIL - Center for Infection and Immunity of Lille, F-59000 Lille, France

[b] Station Biologique de Roscoff, Sorbonne Université, CNRS, UMR 7144, Adaptation et Diversité en Milieu Marin, Place G. Teissier, 29680 Roscoff, France

[c] Observatoire Oceanologique de Banyuls-sur-Mer, UMR 8222 CNRS-SU Laboratoire d'Ecogéochimie des Environnements Benthiques, avenue Pierre Fabre, 66650 Banyuls-sur-mer, France

[d] UMS 2014-US 41- PLBS- Plateforme Lilloise en Biologie & Santé, BioImaging Center Lille (BICeL), Univ, Lille, France.

* Corresponding author. Univ. Lille, CNRS, Inserm, CHU Lille, Institut Pasteur de Lille, U1019 - UMR 9017 - CIIL - Center for Infection and Immunity of Lille, F-59000 Lille, France

*E-mail address:*celine.wichlacz@univ-lille.fr

Boidin-Wichlacz: 0000-0002-0242-868X

Tasiemski: 0000-0003-3559-5115

Andersen: 0000-0003-3962-100X

Hourdez: 0000-0001-6418-3887

Jouy: 0009-0001-4598-6518

Keywords: *Capitella capitata*, erythrocytes, immune function, antimicrobial peptide, globin

ABSTRACT

The polychaete *Capitella* is a typical member of the 'thiobiome', and is commonly used as an eutrophication indicator species in environmental assessment studies. To deal with a sulfide-rich and poisonous surrounding, cells in close contact with the environment, and thus able to play a major role in detoxication and survival, are circulating cells. This work aimed to morpho-functionally describe the circulating coelomic cells of *Capitella* from the English Channel inhabiting the sulfide-rich mud in Roscoff Harbor. In general, worms have three types of circulating cells, granulocytes involved in bacterial clearance and defense against microorganisms, eleocytes with an essentially trophic role and elimination of cellular waste, and erythrocytes which play a role in detoxification and respiration *via*

their intracellular hemoglobin. By combining diverse microscopic and cellular approaches, we provide evidence that *Capitella* does not possess granulocytes and eleocytes, but rather a single abundant rounded cell type with the morphological characteristics of erythrocytes *i.e.* small size and production of intracellular hemoglobin. Surprisingly, our data show that in addition to their respiratory function, these red cells could exert phagocytic activities, and produce an antimicrobial peptide. This latter immune role is usually supported by granulocytes. Our data highlight that the erythrocytes of *Capitella* from the English Channel differ in morphology and bear more functions than the erythrocytes of other annelids. The simplicity of this multi-task (or polyvalent) single-cell type makes *Capitella* an interesting model for studies of the impact of the environment on the immunity of this bioindicator species.

1. Introduction

Capitella spp. are small (*ca.* 1 cm in length) benthic polychaetes belonging to the family Capitellidae. *Capitella* Fabricius, (1780) is generally considered to be a cosmopolitan genus, found from the coastal "thiobiome" (Boidin-Wichlacz et al., 2021) to deep-sea regions (Silva et al., 2016) that are enriched in heavy metals and sulfide, up to levels that are toxic for most metazoans. Reish & Gerlingher (1997) reported that *Ophryotrocha labronica* (polychaete) was the most sensitive more heavy metal contaminants (Reish and Gerlinger, 1997). Changes in the benthic macrofauna community observed after episodes of severe oxygen deficiency indicate differential tolerance to oxygen concentrations (Diaz and Rosenberg, 1995), with mollusks and polychaetes being typically more tolerant to oxygen deficiency than echinoderms, fishes, and crustaceans. Although these types of extreme habitats allow less competition-induced stress, specific genetic, physiological adaptations and peculiar symbiotic associations are needed for the survival and thriving of these constraining biomes (Hourdez et al., 2021). Several studies have now provided evidence that the immune system is an interesting marker to follow the adaptation of annelids to their environment. For instance, a phenotypic switch of the immune coelomic cells is observed in coastal *Hediste diversicolor* populations differentially exposed to heavy metals in their natural habitats (Cuvillier-Hot et al., 2014). The number of coelomic cells producing antimicrobial peptides (AMPs) of the Pompei worm *Alvinella pompejana* decreases as animals are exposed to lethal temperatures, thereby likely affecting the immunity of the animals (Ravaux et al., 2013).

The characterization of coelomocytes in invertebrate aquatic species is a first step in understanding immunological processes. In general, there are three main circulating cell types in the coelomic fluid: granulocytes, eleocytes and erythrocytes (Vetvicka and Sima, 2009). Granulocytes (also called amoebocytes) form the largest category, present in almost all polychaete species studied so far. Granulocytes exhibit a granulated cytoplasm and exert phagocytic, encapsulation and cytotoxic activities (Berlov and Maltseva, 2016; Porchet-Henneré and Vernet, 1992). A second type, called

eleocytes, has often been described as agranular lymphocytes or adipo-spherular cells (Liebmann, 1942). Eleocytes may also be phagocytic and participate in disposing or disintegrating muscle fibers that result from developmental changes during metamorphosis (Baskin, 1974). These free coelomic cells are also considered principal distributors of metabolites during sexual maturation (Fischer and Hoeger, 1993). Eleocytes are not found in all polychaete families, as they are missing in Arenicolidae, Glyceridae, Nephtyidae, and Syllidae (Franchini et al., 2016; Vetvicka and Sima, 2009). The third cell type, erythrocytes (literally red blood cells with a nucleus), is found in a relatively small number of taxonomically diverse invertebrates (Glomski and Tamburlin, 1990). In marine annelids (polychaetes), they have been reported in Capitellidae, Cirratulidae, Glyceridae, Terebellida and Opheliidae (Goodrich, 1898; Jouin-Toulmond et al., 1996). According to Dhainaut and Porchet-Henneré (1988) erythrocytes in polychaetes form two lineages which differ in morphology and functional specialization (Dhainaut and Porchet-Henneré, 1988), such as regeneration or phagocytosis. In most annelid species, erythrocytes are specialized in the transport or storage of oxygen that reversibly binds to intracellular hemoglobin (Seamonds and Schumacher, 1972). However, in certain annelids species possess large extracellular hemoglobin that is capable to bind and transport oxygen, and ensures a significant form of oxygen storage (Hourdez et al., 2000; Weber and Vinogradov, 2001). An investigation comparing the respiratory properties of the erythrocytes between ten sibling species, morphologically similar to *Capitella capitata*, pointed to distinctive and non-overlapping differences in their diameter according to the species. More importantly, the respiratory properties of the erythrocytes are distinctive of most of the species examined, for unclear adaptive reasons (Mangum et al., 1992). Overall, in invertebrate species, however, respiratory pigment properties usually reflect environmental conditions (Weber and Vinogradov, 2001). Hemoglobins (Hb) contained in erythrocytes of a North American population of *Capitella* (likely corresponding to the recently described *C. telata*) have high to moderate oxygen affinities, little or no pH dependence, and no cooperativity. These properties are more typical of oxygen storage globins such as myoglobins. In members of the families Capitellidae, Cirratulidae, Glyceridae and Opheliidae, erythrocytes have been shown to also be capable of active phagocytosis. Unlike eleocytes, however, they primarily unselectively phagocyte foreign material (Stanovova, 2019; Vetvicka and Sima, 2009). However, to date, erythrocytes have not been shown to exert immune functions.

In polychaetes such as Capitellidae and Alvinellidae, inhabiting sulfide rich habitats, hemoglobins may also protect the annelid worms from the toxic action of sulfide by a detoxifying process (Jouin-Toulmond et al., 1996; Terwilliger, 1998; Wippler et al., 2016). Other authors have shown an emerging role for invertebrate intracellular hemoglobins in innate immunity, in bivalves. Purified Tg-HbI and Tg-HbII from the bivalve *Tegillarca granosa* showed antibacterial activities against Gram-negative and Gram-positive bacteria (Bao et al., 2016; Coates and Decker, 2016).

Coelomocytes, and notably granulocytes, are generally endowed with defensive capacities, namely phagocytic, encapsulating, and microbicidal activities that contribute to both cellular and humoral

responses (Cuvillier-Hot et al., 2014). Components that participate in innate immune responses include humoral factors such as antimicrobial peptides toxic for most (AMPs) and lysozyme-like proteins, which are secreted in body fluids. AMPs play an important role, as they are produced constitutively or induced upon infection in coelomocytes, as well as in the body-wall to defend against invading pathogens (Bruno et al., 2019; Wu et al., 2021). In marine polychaetes, such an induction has been shown in the lugworm *Arenicola marina* producing Arenicin-1 and 2, in *Hediste diversicolor* secreting Hedistin, and in the hydrothermal vent *Alvinella pompejana* producing Alvinellacin (Maltseva et al., 2014; Tasiemski et al., 2014, 2004). A putative AMP called Capitellacin has been predicted in *Capitella teleta* based on genomic analysis (Tasiemski et al., 2014). Capitellacin has been recently been shown to possess antibacterial and antibiofilm activities against *E. coli* (Safronova et al., 2022). A lysozyme activity has also been detected in coelomocytes and coelomic fluid of the polychaetes *Arenicola marina* and *Hediste diversicolor* (Cuvillier-Hot et al., 2014; Grossmann and Reichardt, 1991).

The North American species *C. teleta* has attracted attention because it has several typical annelid specificities and exhibits some advantages for developmental and regenerative studies (Boyle et al., 2014; Seaver, 2016; Seaver and Kaneshige, 2006). Genetic studies have revealed that several species of *Capitella* can be found on the shores of Brittany, including one hereafter referred to as *Capitella* C-Channel1 (Boidin-Wichlacz et al., 2021). So far, no study on the immune defense system of this species has been conducted, except studies showing that sequences of the genomes from *Capitella* sp. suggest the existence of Toll-like receptors (TLRs), which are pattern-recognition receptors (PRRs) (Davidson et al., 2008). In this context, the goal of this paper is to investigate the cellular and humoral response immunity of the bioindicator species C-Channel1 using an array of morpho-functional approaches.

2. Materials and methods

2.1. Animals

All described experiments were performed on C-Channel1 (corresponding to *Capitella* C-Channel1 in Boidin-Wichlacz et al. 2021) adults that were collected between 2015 and 2023 in Roscoff (France) (48°42.743’ N, 4°00.092’ W). *Capitella* were collected at low tide. The surveyed sites (an average of 4 sampling points in a 1 m² zone) are enriched in silts, with a high concentration of organic carbon in the Roscoff Harbor (Hourdez et al., 2021). The sediment was sieved on a 500 µm mesh in the field and animals were brought back to the laboratory for sorting under a dissecting microscope. *Capitella* have been reared at Lille laboratory in aquaria containing a 2–3 cm layer of sediment and filled with artificial seawater (Instant Ocean® Sea Salt), equipped with an aeration

system and kept at room temperature (21 °C) as described earlier (Boidin-Wichlacz et al., 2021). To feed the worms, the sediment was regularly supplemented with a mixture of ground commercial dried baby cereal (HiPP Biologique, France).

2.2. Morphological description of the coelomic cells

2.2.1. Observation of the cell types *in situ*

Whole adults (n= 3) were fixed for 4 h in 2.5% glutaraldehyde in 0.2 M sodium cacodylate buffer (pH 7.4) at 4 °C and progressively dehydrated with increasing concentrations of ethanol in water (55% to 100%). They were embedded in a hydrophilic resin (Technovit® 7100, Electron Microscopy Sciences) following the manufacturer's instructions. Ten-µm thick sections were stained for 4 min with toluidine blue at 0.1% in water. Specimens were examined with a Zeiss Stemi 305 stereomicroscope. Images were taken with a camera and the Zen software.

2.2.2. Flow cytometry analysis of the coelomocyte population

Coelomic fluid from 10 animals (for a total volume of 10 µL) was collected using a glass capillary introduced into the coelomic cavity. Cellular samples were analyzed with an EPICS XL-MCL4; Beckman Coulter flow cytometer. During the analytical experiments, 10,000 threshold events per sample were collected, with side scatter for cell complexity/granularity, and forward scatter for cell size. The results were analyzed using the Expo 32 software (Cytometry systems).

Coelomic fluid from 4 heterogeneous batches of 10 individuals were analyzed in spectral experiments with a SONY SP6800 Spectral Cell Analyzer : 5,000 events per sample were collected, with the side scatter providing information about cell complexity/granularity, and the forward scatter for measuring cell size. The acquisition was done with 3 lasers with exciting wavelengths at 488 nm, collinear 405 nm and 638 nm. The emission was recollected by 32 photomultiplier tubes (PMTs) from 500 to 800 nm and 2 more from 420 to 480 nm.

2.2.3. Observation of the cell surface of the coelomocytes by scanning electron microscopy (SEM)

Coelomocytes from five animals (around 5 µL), were fixed with paraformaldehyde 4% in seawater for 1 h, then were dehydrated through an ethanol series (55–100%), critical-point dried, and platinum-coated (20 nm) in a Balzers SCD-030 sputter-unit before observation using SEM (JEOL JSM-840A) at 20 kV accelerating voltage.

2.2.4. Differential staining for light microscopic discrimination of the coelomocyte population

Nuclear staining of the cells with DAPI (4,6-diamidino-2-phenylindole): the cells from 5 animals fixed with paraformaldehyde at 4% in seawater for 1 h were centrifuged on coated slides using a cytocentrifuge at 4,000 rpm for 8 min at 4 °C, and then washed three times with phosphate-buffered

saline (PBS at 0.1 M, pH 7.4) for 10 min and incubated with a DAPI (0.5 µg/mL in PBS) (ROTH) solution in the dark for 20 min at room temperature.

Differentiation between acidic and alkaline vesicles in the cytoplasm of the coelomocytes: 20 mg of neutral red was dissolved in 1 mL DMSO (Sigma), then filtered through Whatman filter paper and diluted 1/5 in PBS. The coelomic fluid from four worms was removed (around 20 µL) and then added to the diluted neutral red solution for 5 min at room temperature. Neutral red stains vacuoles from red (for acidic vacuoles) to yellow (for alkaline vacuoles). The coelomic fluid from four worms was removed for this purpose.

Iron detection related to the presence of hemoglobin in the coelomocytes: Coelomic fluid of the animals (around 5 µL, n= 5 individuals) deposited on a Superfrost glass slide (cytocentrifuged at 4,000 rpm for 8 min at 4 °C) was immersed with Perls reagent (2% potassium ferrocyanide and 2% hydrochloric acid) for 30 min. Ferric ions then produce Prussian blue, an insoluble blue compound. The slides were thoroughly rinsed in distilled water for 5 min. The counterstain was carried out with a modified Harris hematoxylin solution according to Mayer (Sigma) for 5 min.

Coelomocyte populations were examined using optical microscopy (Zeiss Axio Imager M2) and images were taken with a camera and using the Zen Microscopy software (Zeiss). Using Image-J software on microscopic pictures, we measured length, width and surface area of stained and unstained cells in suspensions, placed on glass slides and covered with a 24 x 50 mm coverslip.

2.2.5. Ultrastructural study of the coelomocytes by transmission electron microscopy (TEM)

The cells of five animals were collected as indicated in section 2.2.2, and immediately fixed according to the protocol previously described (Boidin-Wichlacz et al., 2012). Cells were dehydrated with ethanol and embedded in Epon (polymerization at 60 °C for 48 h). Ultrathin sections (80–90 nm) were made from the Epon blocks, placed on 200-mesh copper grids, and stained with uranyl acetate and lead citrate with a standard protocol. Specimens were observed with a Hitachi H 600 electron microscope.

2.3. Molecular identification of hemoglobin from Capitella C-Channel1

2.3.1. RNA extraction

The total RNAs of each group, with 10 individuals per condition were extracted with the TRI-Reagent solution (Sigma), following the manufacturer's protocol. The concentration of extracted RNA was measured with the Qubit® RNA HS kit and the Qubit® 3.0 Fluorometer.

2.3.2. cDNA synthesis

Complementary DNA (cDNA) synthesis using the RT-PCR System protocol (Fermentas, Thermo Fisher Scientific Inc) was performed according to the manufacturer's instructions with 1.2 µg of RNA

per sample. Controls RT Amplification was carried out with GoTaq® G2 DNA Polymerase (Promega). Reaction mixtures contained 10 µmol.L^{-1} of each primer, 10 µmol.L^{-1} of each deoxynucleotide triphosphate, 5X Go Taq® Flexi green buffer (Promega), and 5 U of GoTaq G2 Flexi DNA polymerase (Promega). The final volume was adjusted to 50 µL with sterile water. The PCR program involved an initial denaturation step at 95 °C for 3 min, followed by 39 cycles of 95 °C for 30 sec, 60 °C for 30 sec, and 72 °C for 30 sec, with a final elongation step at 72 °C for 5 min. Primers used for the semi-quantitative PCR were designed with the Primer3 Input software (http://primer3.ut.ee/). Hemoglobin, F5'-GAAACCGGTCGTCTAAATCA-3', R 5'-CCATGATGATTGTTGAAGTT- 3'.

2.3.3. Cloning and sequencing

The PCR products were purified with the Nucleospin Extract Kit (Macherey-Nagel) and cloned in the TA Cloning kit (Promega), according to the protocol provided by the manufacturer. DNA plasmids were Sanger-sequenced with the FM13/RM13 universal primer using the BigDye Terminator kit (Applied Biosystems, Foster City, CA).

2.3.4. Sequence analysis

The nucleotide sequences were translated into amino acid sequences using the universal genetic code with the Expert Protein Analysis System (http://www.expasy.org/). The resulting sequences were used for BLASTP searches on the NCBI website (http://www.ncbi.nlm.nih.gov/blast) to recover similar sequences for phylogenetic studies. The sequences resulting from amplification were deposited in the GenBank database under the accession numbers MT577032 for hemoglobin. The deduced amino acid sequences were aligned with the corresponding sequences from various animals using the ClustalW software. Based on this alignment, an UPGMA tree was constructed using the Mega-X software package (http://www.megasoftware.net). The analyzed globin sequences were retrieved from GenBank along with the 17 intracellular globin sequences from the genome of *Capitella teleta*, four sequences from the genome of *Lumbricus terrestris* and three sequences from the genome of *Platynereis dumerilii* identified by Song et al. (Song et al., 2020). All accession numbers are listed in Table 1.

2.4. Investigation of phagocytic activity of the coelomocytes

2.4.1. Phagocytic activity

For each individual (n=10), toluidine blue-stained *Saccharomyces cerevisiae* (Baker's yeast type II), were used as target cells for phagocytosis. Two hundred and fifty milligrams of *S. cerevisiae* were suspended in 5 mL of PBS with 8% glucose (PROLABO) containing 1% toluidine blue (ROTH). The suspensions were then washed twice by centrifugation at 3000 g, 4 °C (for 5 min per wash). After

gently mixing, the tube was incubated for 4 h at RT. Phagocytosis was quantified and qualitatively analyzed through morphological examination. All the samples were counted under a microscope (Axio lab A1, Zeiss) with a camera and the Zen 2011 module (Zeiss) for image analysis. Results are expressed as the percentage of phagocytic cells.

For each experimental individual (n=10), a volume (about 10 µL) of cells was mixed at a ratio of 50 bacteria per cell with *Vibrio alginolyticus* (Urakawa and Rivera, 2006) and *Bacillus hwajinpoensis* (Cuvillier-Hot et al., 2018) are bacteria typical of the habitat where the annelid worm species is living. Bacteria were labeled with Fluorescein-5-isothiocyanate (FITC; Interchim, France) by incubating 109 bacteria per ml in a solution of 0.01 mg of FITC per mL, 0.1 M sodium carbonate at pH9.6, for 1 h at 25°C and then washing the bacteria three times with phosphate-buffered saline (PBS). After gently mixing, the tube was incubated for 1.3 h at RT. After incubation, each sample was fixed in paraformaldehyde 4% and stored at 4 °C. Part of the samples were further processed by FACS (Fluorescence Activated Cell Sorting). The other part of the samples was used for confocal microscopy analysis. To distinguish phagocytotic cells, we used the double-fluorescence technique of labeling the bacteria with FITC and the SYTO 60 red (Invitrogen) fluorescent nucleic acid stain after cell fixation. Fixed cells are diluted with 200 µL of PBS. Samples are placed in the cytospin (Thermo Scientific® Cytospin® 4 Cytocentrifuge) for 4min at 2000 rpm. The smears on the slides are covered with a solution of SYTO 60 diluted 1/3000 for 15 min at room temperature. After two 10 min rinses with PBS, the slides were observed under a confocal microscope. Confocal images were acquired with a line scanner microscope (LSM880, Zeiss) through a 63x objective lens (Plan-Apochromat 63x/NA 1.4 oil immersion). A z-stack image was recorded with a voxel size of 0.085 µm*0.085 µm*0.369 µm. SYTO 60 was excited with a 633 nm laser, and its fluorescence was measured between 643 and 720 nm. The FITC signal coming from the bacteria was excited with an argon laser at a wavelength of 488 nm, and the fluorescence was collected between 500 and 544 nm. 3D rendering and orthogonal views were obtained with the Imaris software (Oxford Instruments, 10.0.1 version). A phagocytosis experiment with yellow latex beads of 1 µm in diameter, at a ratio of 5 beads per cell (Fluoresbrite Plain YG 1.0 Micro Microsphere, Polysciences) are presented in supplementary data. Phagocytic activity of the coelomocytes at 1.3 h after adding the beads was estimated as the percentage of fluorescent events detected by the cytometer in the gates corresponding to the cell populations.

2.4.2 Analysis of flow Cytometry Phagocytosis Data

The data were extracted from the SP6800 instrument, without any spectral unmixing, to keep the autofluorescence of the cells. The acquisition data were analyzed with the Kaluza software (BeckmanCoulter v2.2). The strategy was to draw a region in FSC/ SSC which excluded the bacteria; this exclusion was checked with the tube with labelled bacteria. In this gating region we observed the fluorescence corresponding to cells labelled by phagocytosis with FITC. Red fluorescence emission helped to identify cellular autofluorescence from the coelomic fluid.

2.5. Identification and function of immune effectors: lysozyme and other antimicrobial peptides

2.5.1 Lysozyme expression

The total RNAs of each group, with 10 individuals per condition were extracted with the TRI-Reagent solution (Sigma), following the manufacturer's protocol. The concentration of extracted RNA was measured with the Qubit® RNA HS kit and the Qubit® 3.0 Fluorometer. The ADNc synthesis was carried out as described in paragraph 2.3.2. Primers used for the semi-quantitative PCR were designed with the Primer3 Input software (http://primer3.ut.ee/). The nucleotide sequence encoding Lysozyme was identified in the *C. teleta* Joint Genome Institute (JGI) database. The specific primers used: Lysozyme, F5-′CCTCTGCGAGCTTCACCTAC-3′, R5 -ATGGAAGGTACTGCACAGGG-3′. The PCR production, loaded on an agarose gel, revealed a single band of the expected size, which was purified with the Nucleospin Extraction kit (Macherey-Nagel), and cloned in TA Cloning kit (Promega) according to the protocol provided by the manufacturer. DNA plasmids were Sanger-sequenced with FM13/RM13 universal primers using BigDye Terminator (Applied Biosystems, Foster City, CA). The resulting sequences were used for BLASTP searches on the NCBI website (http://www.ncbi.nlm.nih.gov/blast) to recover similar sequences for phylogenetic studies. The sequences resulting from amplification were deposited in the GenBank database under the accession numbers MT577031 for the lysozyme. The deduced amino acid sequences were aligned with the corresponding sequences from various animals using the ClustalW software. Based on this alignment, an UPGMA tree was constructed using the Mega-X software package (http://www.megasoftware.net). Since lysozyme activity has been demonstrated for i-type proteins belonging to both deuterostomes (echinoderms) and protostomes (mollusks and annelids), all the analyzed sequences of different types of lysozymes-i were retrieved from GenBank. All accession numbers are listed in Table 1.

2.5.2 Lyso-plate assays

Enzymatic activity was measured using the *M. luteus* lytic assay (*Micrococcus lysodeikticus*, Sigma) as described by Osserman and Lawlor (Osserman and Lawlor, 1966). Assays were performed on pools of whole three animals and of coelomic fluid collected from three animals. In this assay, the diameter of the cleared zones is proportional to the concentration of lysozyme. The diameters can be measured directly and compared to the diameters obtained with standard solutions of lysozyme for quantification (expressed in $mg.mL^{-1}$).

2.5.3 Microbial challenge

Forty adults were sorted into two groups, and each of these groups processed into two batches: the control individuals and the microbial-challenged individuals. For the first group, whole animals were used. For the second group, only coelomocytes were used. The four groups (n= 10 each) were

transferred into boxes containing 2 mL seawater enriched with a cocktail of live bacteria (*Vibrio alginolyticus* and *Bacillus hwajinpoensis* at $1x10^5$ CFU/mL) for 16 h at room temperature. *Vibrio alginolyticus* and *Bacillus hwajinpoensis* are bacteria typical of the habitat where worm species is living. A control experiment under the same conditions but without the addition of the cocktail of live bacteria was also carried out. All these experiments were carried out in triplicate.

2.5.4 Gene expression of lysozyme and other AMPs on whole animals and coelomocytes

Lumbricin (GenBank : ELU06641.1) and Capitellacin (GenBank : AMQN01012506.1), both AMPs previously described, seem to be interesting candidates for AMPs search. The nucleotide sequence encoding Lumbricin was identified in the *C. teleta* Joint Genome Institute (JGI) database. The total RNAs of each group, with 10 individuals per condition were extracted with the TRI-Reagent solution (Sigma), following the manufacturer's protocol. mRNA of cells from 10 animals, was isolated with the Dynabeads® mRNA DIRECT™ Micro Kit (Ambion, Life technology). RT reactions were performed as described in the previous section (section 2.3.2). Primers used for the semi-quantitative PCR were designed with the Primer3 Input software (http://primer3.ut.ee/). Lumbricin: F5′-GCTAAGAGGATTCGGGCTTG-3′,R 5′-CTCATCTGCGGCATTAGCTG-3′; expected product size 130 bp. Lysozyme: F5′-CCTCTGCGAGCTTCACCTAC-3′, R5′-ATGGAAGGTACTGCACAGGG-3′; expected product size 243 bp. Capitellacin: F 5′-ATCATGGTTACTGGCGTCGT-3′, R 5′-CGTCAAATGAGGCGGAAGTA -3′; expected product size 490 bp. Amplification for sequencing used the same PCR conditions as described in the previous section, but the 5X Go Taq® Flexi green buffer (Promega) was replaced by an unstained buffer to prevent interference with cloning. Success of amplification was evaluated by electrophoresis in a 1.5% agarose gel. The cDNA obtained was used to quantify the relative quantity of lysozyme-like, Lumbricin, and Capitellacin mRNA compared to GAPDH (GlycerAldehyde-3-Phosphate DeHydrogenase) (protein ID :159122 from the JGI Genome site) mRNA, used as reference (F 5'-GATGGCAAGATGAAGGGATTC and R 5'-AGAGCAATGCCTGCCTTG-3').

2.5.5 Immuno-localization of Cc-Lumbricin and Cc-Capitellacin by immunohistochemistry

Bacterially challenged and non-challenged *Capitella* worms were fixed in paraformaldehyde (4% in filtered seawater at 4 °C) for 4 h. A region of Capitellacin (LGAWLAGKVAGTVATYAWNRYV) was chemically synthesized, coupled to Ovalbumin and used for the immunization procedure of two New Zealand White rabbits (Saprophyte Pathogen free) according to the protocol of CovalabTM (France). The polyclonal anti-Lumbricin antibody is the one described in (Schikorski et al., 2008). Immunohistochemistry on 7-µm thick paraffin sections on adult tissues was performed with the rabbit Capitellacin antiserum (1:400) and the rabbit Lumbricin antiserum (1:400) and the FITC-conjugated anti-rabbit secondary antibody (1:100; Jackson Immunoresearch Laboratories). Nuclear staining of the cells using DAPI was also carried out, as described above. Samples were examined using a

fluorescence microscope equipped with the ZEISS Axio Imager 2 software, allowing us to merge images captured under different wavelengths.

2.5.6 Sodium Dodecyl Sulfate PolyAcrylamide Gel Electrophores (SDS-PAGE)

Mucus from challenged and unchallenged *Capitella* (as described in the section "Microbial challenge") was recovered using a sterile swab. The protein concentrations of the mucus extract and of the whole animal were determined using a protein–dye binding assay kit (Bio-Rad Laboratories, CA, USA) based on the Bradford protein analysis method (Bradford, 1976). Bovine gamma globulin was used as a standard. Proteins were separated by denaturing SDS-PAGE electrophoresis. The running gel was composed of 12% acrylamide (12% acrylamide; Tris-HCL 1.5 M, pH 8.8; 0.1% SDS; 0.1% ammonium persulfate; 0.01% TEMED) and the stacking gel was composed of 4% acrylamide (4% acrylamide; Tris-HCL 0.5 M pH 6.8; 0.1% SDS; 0.1% ammonium persulfate; 0.01% TEMED). A total of 57 µg of protein was loaded in Laemmli buffer (Tris 125 mM pH 6.8; 20% glycerol; 4% SDS and 5% β-mercapto-ethanol). Gels were run at 70 V for 15 min and then at 130 V for 60 min.

2.5.7 Western blot

The proteins of the SDS-PAGE gel were transferred to a 0.2 µm nitrocellulose membrane (Bio-Rad) by semi-dry electroblotting (0.8-1.2 mA/cm²). After transfer, the gel was stained by Coomassie Brilliant Blue R-250 (Bio-Rad), to check that protein transfer to the membrane was complete. The membrane was blocked for 1 h in PBS at 0.1 M containing 0.05% Tween 20 and 5% casein and was then probed with the rabbit polyclonal anti-Lumbricin and anti-Capitellacin antibodies (1:1000 dilution) in the blocking solution (PBS at 0.1 M with 5% w/v nonfat dry milk) overnight at 4 °C. After three washings with PBS / 0.05%-Tween 20, the membrane was incubated for 1 h in the blocking solution at room temperature with the peroxidase-conjugated anti-rabbit secondary antibody Abcam (1:5000 in PBS at 0.1 M containing 0.05% Tween 20; at 1 h). A ClarityTM Western ECL Substrate (Bio-Rad) was used to visualize the chemiluminescence of the immunolabelling with a Kodak Bio Max light film.

3 Results

3.1 A single small-sized cell population in the coelomic fluid of Capitella C-Channel1

Analysis by flow cytometry (Fig. 1) shows a cloud of red dots, each of which represents a single cell that has passed through the instrument (Fig. 1A, Gate1). Based on differences in their physical parameters (Forward Scatter (FSC) and Side Scatter (SCC)), a single population was detected. The existence of a single cell type was also confirmed by the morphological observations of these cells. First on sections of whole animals stained with toluidine blue (Fig. 1B), a non-specific, basic dye with

a good affinity for acidic structures such as nucleic acids (ribosomes, nucleus and endoplasmic reticulum).

Zooming in on these cells showed they had a round or oval shape with an eccentric nucleus surrounded by a wide cytoplasm with acidic affinity (Fig. 1C). Observed with no fixative on a glass slide, the coelomic cells naturally appeared all red in color (Fig. 1D), numerous ($1.3\ 10^7$ cells.mL^{-1}) and small. Measurements made on cells stained with various non-fluorescent stains had a Ferret's diameters of 9.12 to 9.31 µm, whereas DAPI fluorescence and unstained cells showed a fuzzier limit, which resulted in Ferret's diameters of 11.69 and 12.61 µm, respectively (see Table S1 in Supplementary material).

Scanning electron microscopy showed the coelomocytes have a relatively smooth surface (Fig. 1E). The structural analysis showed a nucleus that was regular in outline (Fig. 2A). A residual body with electron-dense contents was also present in the cytoplasm, well-rounded in appearance, and with a diameter of 1 µm (black arrow on Fig. 2A and white arrow on Fig. 2B). The perinuclear cytoplasm contained mitochondria and a few vacuoles (Fig. 2C). Staining by neutral red was observed in the cell as either an orange-yellow coloration (indicating a rather acidic affinity) within small vesicular compartments (white arrow on Fig. 2D). The alkaline residual body exclusively stained bright pink (black arrow on Fig. 2D).

3.2 The coelomocytes are erythrocytes containing intracellular hemoglobin

Perls' stain of the cells showed an iron deposit visible as a bright blue granular staining (black arrow, Fig. 3A). In addition to accumulating iron metal, all coelomocytes were naturally colored by a red pigment present inside, presumably a respiratory pigment (Fig. 3C). RT-PCR using hemoglobin primers combined with nucleotide sequencing allowed the molecular identification of a hemoglobin-like protein transcript from the cells of *Capitella* (Fig. 3B). The spectra with 488nnm excitation are relatively similar (Fig. 3D). But with the others excitations, 405 and 638 nm, we have spectra with different intensities of red fluorescence, which could better correspond to different amounts of hemoglobin. This allows us to assume that in the mixture there are populations with different amounts of hemoglobin. This difference is very clear in figure 3E in the form of 2 spectra; the red arrow indicates the spectrum with a higher intensity, thus a greater content of hemoglobin, than the spectra indicated by the black arrow. This difference varies with different animal batches (Supplementary material, Fig S1). The animals are therefore not homogeneous in their quantity of hemoglobin.

To better understand the origin of the globin found in the coelomocytes of C-Channel1, we carried out a phylogenetic analysis using representatives of the diversity of globins found in annelids. This dataset includes representatives of the typical intracellular globins, extracellular globins, as well as myoglobins, neuroglobins, and the unusual polynoid extracellular hemoglobins (Belato et al., 2020; Projecto-Garcia et al., 2017; Weber and Vinogradov, 2001) present in various annelid species. We

produced a maximum-likelihood phylogenetic tree with this sampling of 51 protein sequences (Fig. 4). The globins fall into two well-supported (100% bootstrap) main groups: (1) the typical annelid extracellular globins and (2) the intracellular globins (myoglobins, neuroglobins and erythrocytic globins), along with the unusual polynoid extracellular globins. All the *Capitella* sequences fall well within the intracellular globins lineage, and the C-Channel1 globin clusters with other intracellular globins from *Capitella teleta* (sequences extracted from the genomic data), with very high confidence (99% bootstrap). Because of the presence of circulating intracellular globin, the coelomic cells of C-Channel1 can be designated as erythrocytes.

3.3 Erythrocytes with phagocytic activity

Erythrocytes incubated with Toluidine-blue-colored yeast cells for 4 h showed an ability to phagocyte up to 10% of yeast cells (Fig. 5A). Flow cytometry analysis was also performed (Fig. 5B, 5C and 5D) on cells incubated for 1.3 h with FITC labeled bacteria or yellow latex beads (Supplementary material, Fig. S2). In figure 5B, the left SSC plot shows non-labelled bacteria with 6% of background autofluorescence (in the frame B). Compared to this, the right-hand plot with the FITC-labeled bacteria are positive at 98% (in the frame B). On figure 5C and D in the left columns, the FSC/SCC plot allows us to frame a region A within the cell-size range which excludes the smaller debris and the majority of the bacteria. When the cells have been in contact with labeled bacteria (Fig. 5D) the cells region A shows a slight modification of the SSC and thus of the complexity or granularity of the cells (SSC). Gated on this Region A, the right columns of figures 5C and D shows the FITC / red emission plot as function of FITC, to contrasts the non-labeled cells (Fig 5C right) and the cells in contact with FITC bacteria (Fig. 5D right). The cells in region C-- correspond to the part of biggest bacteria which could be in region A (on the FSC/SSC plot, Fig 5C, left column) but they are completely negative for the red emission. The autofluorescence of bacteria is lower than the coelomic fluid cells in the red emission. So the animals cells of interest are in the upper part of the plot : in the C-+ region the cells are positive for the red emission but negative for the FITC fluorescence. In the C++ region the cells are positive for the red emission and for FITC fluorescence : it represents 0.64% for the non-labeled cells and 4.38% for the cells in contact with the FITC bacteria : cells that have phagocytosed the bacteria . The test of phagocytic activity revealed that the erythrocytes had ingested up to 3.74% of the labelled bacteria (Fig. 5D) and the phagocytosis is mainly present in cells with low hemoglobin levels (red square). Similar percentage of ingestion was obtained with yellow latex beads (Fig S2). Figure 5E shows the engulfment of labelled bacteria by an erythrocyte. Image of confocal optical sections of a phagocytic erythrocyte in xyz and xz planes (Fig. 5F) shows marked bacteria within the cell cytoplasm.

3.4 Capitella C-Channel1 erythrocytes produce an AMP but no Lysozyme

At first, lysozyme (GenBank ID MT577031) from C-Channel1 (*Cc*) was molecularly identified by RT-PCR combined with cloning and nucleotide sequencing. A phylogenetic analysis on lysozyme comparison with other deuterostome and protostome sequences from seventeen species (Fig 6A) was carried out. The distance tree obtained showed that the analyzed annelid sequences form a distinct lineage including destabilase I from *Hirudo medicinalis*, with the exception of *Caenorhabditis elegans* sequence lysozyme-i. Lysozyme-like C-Channel1 seems to be closely related to the lysozyme of the North American species *Capitella teleta.* An activity able to lyse *M. lysodeikticus* cell walls was detected in whole *Capitella* worms, after an overnight incubation at 37°C. A clear ring of lysis, 12 mm in diameter was observed in animals stimulated (ab) by bacteria, for a diameter of 0.8 mm only in unstimulated animals (a). No lytic activity was observed in the coelomic cells (Fig. 6B). After adults had been exposed to a high load of live environmental bacteria (*V. alginolyticus* and *Bacillus hwajinpoensisat)*, the transcripts of lysozyme were detected by semi-quantitative RT PCR in the whole animals (Fig. 6C, lane a), but not in their coelomocytes (Fig. 6C, lane c) confirming that the erythrocytes do not express the lysozyme gene. When the *Capitella* worms were microbially challenged, they expressed the lysozyme more intensely (Fig. 6C, lane ab), while the challenged coelomocytes still did not express it (Fig. 6C, lane cb).

The gene expression patterns of the lysozyme-like, *Cc*-Lumbricin, and also *Cc*-Capitellacin were then investigated by semi-quantitative RT-PCRs first in the whole individuals challenged and unchallenged by bacteria, and secondly in the erythrocytes collected from bacterially challenged or unchallenged *Capitella*. As presented in figure 7A, only *Cc*-Capitellacin was produced by the coelomocytes. The cellular gene expression of this AMP was even increased when the worms had been exposed to bacteria. The other AMP (*Cc*-Lumbricin) (Fig. 7A) was not produced by the erythrocytes, and as observed for the lysozyme, the transcripts were detected in the bacterially challenged animals. Western blot analyses were performed on the same tissues from the same whole individuals and their mucus. The known molecular mass of Lumbricin I is 7.2 kDa, and 6.7 kDa for *Hm*-Lumbricin. The Western blot showed a 10 kDa band in the *Capitella* worm's mucus, which likely corresponds to the Cc Lumbricin (Fig.7B). The Western blot analysis (Fig. 7C and 7D) confirmed the synthesis of the peptide, Capitellacin, but also showed a band of slightly greater molecular weight than expected. The band detected at less than 17 kDa could be the precursor of Capitellacin.

Immunohistochemistry using the anti-*Hm*-Lumbricin (Fig. 8A to 8D) and the anti-Capitellacin (Fig. 8F to 8G) were performed and also supported the RT-PCR and Western Blot results. Controls were performed with pre-immune serum (Fig. 8C, C1 and H, H1). *Cc*-Lumbricin was detected under basal (no exposure) conditions (Fig. 8A), the peptide was immunodetected in the digestive tract (Fig. 7A) and integument (Fig. 8A1). Interestingly, the immune staining for *Cc*-Lumbricin was most strongly observed in the tegument after bacterial challenge (Fig. 8B1). We observed an immunodetection of bacteria trapped within the mucus of challenged animals (Fig. 8D), confirming the observation of *Cc*-

Lumbricin produced in mucus secretion by Western blot (Fig. 7C and 7D). The Capitellacin-like peptide (*Cc*-Capitellacin) was immunodetected under basal conditions in the digestive tract (Fig. 8F), that immune staining for *Cc*-Capitellacin was strongest in the tegument after bacterial challenge (Fig.8G). The *Cc*-Capitellacin peptide was also detected in the erythrocytes (Fig. 8F1), but after bacterial challenge only (Fig. 8G1).

4. Discussion

Coelomocytes present in the coelomic fluid of all polychaetes are usually heterogeneous in morphology, size, relative abundance, and function, which makes a single standard classification a difficult task. Nonetheless, it is rare to describe a single type of cell in the coelomic fluid with various functions. In the polychaete *Glycera dibranchiata* the only population described in the coelomic fluid was mainly studied for its intracellular hemoglobin (Seamonds and Schumacher, 1972). Dales (1964) described a single type of coelomocytes in *Amphitrite johnstoni*, while earlier writers described 3 types of cells in the coelomic fluid of that species (Dales, 1964). There are three types of coelomocytes described for *Arenicola marina*, but these cells are likely to represent the early stages of differentiation of granular integrations: with a change in physiological state, granules can appear and accumulate. The distribution of granular cells depends on the age and sex of the animal and is also correlated with the stage of maturation of sex products (Persinina and Chaga, 1994). Based on our study, we conclude that a single cell-type is present in the coelomic fluid of adults C-Channel1.

Furthermore, the detection of intracellular hemoglobin within these coelomocytes makes it possible to classify them as erythrocytes. The size of C-Channel1 erythrocytes is similar to that of *Alvinella pompejana* erythrocytes (10.78 ± 2.15 µm, n=98) (Jouin-Toulmond et al., 1996), however in the Terebellidae family erythrocytes are larger, measuring about 20 µm (Terwilliger et al., 1985). The erythrocytes of C-Channel1 have a regular shape, which contrasts with erythrocytes from *Amphitrite ornata* and *Enoplobranchus sanguineus* (Glomski and Tamburlin, 1990).

A study on erythrocytes oxygen binding capacities in capitellid polychaetes shows that it is generally species-specific, and the authors suggest that the differences may prove to be adaptations to thermal properties of their environment, to their body size, or both (Mangum et al., 1992). The presence of high-affinity hemoglobin and oxygen-combining capacities has been shown in the coelomic fluid of *Capitella capitata* of the Yeahn Estuary in Devon (Wells and Warren, 1975). The ultrastructure of the large (20 µm diameter) erythrocytes from *Pista pacifica* observed with transmission electron microscopy shows a homogenous gray electron-dense cytoplasm that is believed to be hemoglobin (Glomski and Tamburlin, 1990). Compared to *P. pacifica*, the small erythrocytes of C-Channel1 do not contain lipid granules, and the electron-dense material is much finer and homogeneous. Song et al. (2020) have identified 17 intracellular globin paralogues, all closely related, in the genome of *Capitella* spI (*C. teleta*) and no extracellular globin. They suggest that the ancestral annelid

extracellular hemoglobins were secondarily lost and replaced by red blood cell globins. Our BLAST analysis revealed that the intracellular hemoglobin amino acid sequences of C-Channel1 matched those of intracellular hemoglobin from *Capitella teleta*. Spectral scans of erythrocytes studied in the wavelength range of 500-650 nm, where the fluorescence spectra are mainly emitted by the hemoglobin, show variability, perhaps due to exposure to hypoxia, age, size or sexual maturity of the individuals. We have demonstrated the presence of lighter-colored animals in C-Channel 1population (Boidin-Wichlacz et al., 2021). The hemoglobin from the annelid polychaete *Glycera dibranchiata*, present in coelomic erythrocytes, was demonstrated to be of a heterogeneous (Seamonds et al., 1971). It is possible that the electron-dense body observed in C-Channel 1 erythrocytes also contained hematin, as shown for the erythrocytes from *Urechis* and those from *Alvinella pompejana* (Jouin-Toulmond et al., 1996). Jouin-Toulmond et al. describe the large dense bodies *Paralvinella* and *Alvinella* as by-products of hemoglobin synthesis combined with iron. *Alvinella pompejana*, is exposed to strong hypoxia and high sulfide concentrations. Under these conditions, the oxidation of hydrogen sulfide could occur everywhere in the coelom. Hematin was present in the granules, it can catalyze oxidation of sulfide and may thus protect the animals from sulfide poisoning. This feature could contribute to the success of *Capitella* spp. in sediment of eutrophicated areas that are often anoxic and highly sulfidic, due to anaerobic bacterial degradation of organic matter. Hemoglobin and sulfide affect one another in several ways. Hemoglobin derivatives are also probably present, explaining the variations in hemoglobin spectra. The formation of sulfhemoglobin has been observed in annelids from sulfide-rich environments (Abele-Oeschger and Oeschger, 1995; Zal et al., 1998). Methemoglobin has been clearly demonstrated in the annelid *Arenicola marina* (Abele-Oeschger and Oeschger, 1995; Bailly and Vinogradov, 2005; Hourdez et al., 1999), which showed that methemoglobin formation occurred with a concomitant liberation of hydrogen peroxide, a potent oxidizing agent which can oxidize sulfide. Nonetheless, other strategies have also been suggested exposed to high sulfide concentrations, including an epibiosis with the giant bacteria *Thiomargarita* sp. which has been shown to be advantageous for the survival of *Capitella* spp. facing seasonal increases of free sulfide in the sediments (Hourdez et al., 2021).

In the morphological examination of the erythrocytes, we observed the presence of vacuoles. Although some small vacuoles and vesicles may be involved in pinocytosis, we have no direct evidence for this or other functions of these organelles. However, the small number of polyribosomes seen in many of the erythrocytes examined, suggests that protein synthesis is occurring at a low level as described for *Glycera dibranchiata* and *Glycera abranchiata* erythrocytes (Glomski and Tamburlin, 1990; Seamonds and Schumacher, 1972). Patterns of cytoplasmic organelle development and distribution observed in certain invertebrate erythrocytes are diverse. The holothurian *Eupentacta quinquesemita* retains a considerable quantity of cytoplasmic organelles throughout their existence in these hemocytes (Fontaine and Hall, 1981). But other patterns have been observed, in some invertebrate erythrocytes which reach a maximal complement of cytoplasmic structures at the peak of synthetic

activity followed by its reduction to a lower level which persists throughout the life-span of the cell (Fontaine and Lambert, 1977). One wonders whether this phenomenon also occurs at C-Channel1 erythrocytes with partial or total removal of cytoplasmic structures such as lysosomes, rough endoplasmic reticulum, polyribosomes and Golgi apparatus.

In most coelomate invertebrates (e.g., molluscs, annelids, arthropods, echinoderms, and tunicates), some of the blood cells are phagocytic. In polychaetes, active phagocytosis has often been experimentally examined by injecting small particles such as ferritin or Indian ink, which are taken up by endocytosis and stored inside vacuoles of the coelomic cells. In C-Channel1 we have shown 10% phagocytic for yeast and 3.7% for labeling bacteria. The same percentage was evaluated for phagocytosis of latex beads (supplementary data). Erythrocytes described in *Glycera siphonostoma* by Goodrich (1898) also ingest foreign particles, and would therefore be actively phagocytic (Goodrich, 1898). *Amphitrite johnstoni* has also been cited as having erythrocytes that appear phagocytic (Glomski and Tamburlin, 1990). The erythrocytes found in C-Channel1, as in *S. alveolata*, would exhibit endocytic activity (Meyer et al., 2021). Capitellid appear monophyletics and phylogenetically as a sister taxa to the *Echiurian spoonworms* (Bleidorn et al., 2003; Kobayashi et al., 2022). Their basal position in the annelid tree might account for the pluripotency of their erythrocytes, rather than having a great diversity of specialized cell types, as more evolved annelids.

Lysozyme activity is a phylogenetically conservative humoral mechanism that has been studied in several classes of invertebrates. In most cases lysozyme activity was detected in the coelomic fluid of the studied species of annelids, rarely exclusively in coelomocytes. We were not able to detect lysozyme activity at the erythrocyte level, but we have demonstrated lysozyme activity and humoral defense process by protein synthesis in response to *V. alginolyticus* and *B. hwajinpoensisat* in the whole animal. BLAST analysis revealed that the lysozyme amino acid sequences of C-Channel1 matched those of Lysozyme protein of *Capitella teleta* (whose lysozyme activity has not been evaluated), with 89% identities, but also 62% amino acid similarities with Destabilase 1 of *Hirudo medicinalis* (Zavalova et al., 2012). This lysozyme may turn out to be a destabilase-lysozyme with both lysozyme and peptidase activity, which has yet to be demonstrated.

By now, several Lumbricin homologs have been identified and described from other polychaetes (Bodó et al., 2019; Cho et al., 1998; Li et al., 2011) and leech species (Schikorski et al., 2008). In *Eisenia andrei* earthworms, the highest expression of *Ea*-Lumbricin mRNA appears in the proximal part of the intestine, while other tested organs, such as coelomocytes, have moderate or low levels (Bodó et al., 2019). We localized the expression of the Cc-Lumbricin mainly in the body wall of C-Channel1 by RT-PCR analysis and by immunohistochemistry. Lumbricin-like antimicrobial peptides named Lumbricin-PG and PP-1 were isolated from skin secretions and coats the epithelial surface of earthworms (Li et al., 2011; Wang et al., 2003). Based on the environments of life of *Capitella* sp., it is rational to think that there are effective anti-infective agents in its skin secretions and epidermis, similar to the earthworms. The results of RT-PCR analysis and Western blot, these findings demonstrate the idea that Cc-Lumbricin

coats the epithelial surface of C-Channel1 whole body, where it might contribute to its first line protective barrier.

AMPs, such as Arenicin from *Arenicola marina* (Ovchinnikova et al., 2004), Perinerin from *Perinereis aibuhitensis* (Weidong et al., 2003), Hedistin from *Hediste diversicolor* (Tasiemski et al., 2007), and Alvinellacin from *Alvinella pompejana* (Tasiemski et al., 2014) are predominantly expressed in coelomocytes. To date, coelomocytes containing AMPs were identified as granulocytes or hyaline cells, but no AMP has been identified in erythrocytes. The highest expression levels of *Cc*-Capitellacin were detected in stimulated *Capitella* worms and their coelomocytes. In C-Channel1 the erythrocytes are likely to produce and secrete *Cc*-Capitellacin into the coelomic fluid, where it exerts its antibacterial activities, thus activating the second line of defense when microorganisms penetrate the body.

Some authors have suggested that the internal heterogeneity of eleocytes, granulocytes, or red-blood cells is related to the presence of different stages of differentiation of a single cell lineage in the whole coelomic fluid. Modern integrated annelid research focuses primarily on the structure and functions of specific proteins, especially antimicrobial peptides. In these studies, little attention is paid to the morphology and classification of whole cells.

5. Conclusions

Based on their morphology and their shared functions, the coelomocytes of *Capitella* C-Channel 1 appear to belong to a single cell type, the erythrocytes. This cell type is primarily involved in respiration. Our study shows they also have a role in phagocytosis and production/secretion of AMP. A Lysozyme-like activity has been detected in whole animals, but not at the erythrocyte level. The presence of Lumbricin analog and Capitellacin analog *(Cc*-Lumbricin and *Cc*-Capitellacin) in the mucus covering the epidermis of the whole animal or in coelomocytes, demonstrates that the distribution and functioning of AMPs in C-Channel1 share some features with AMPs from other annelids.

Author contributions

Céline Boidin-Wichlacz and Aurélie Tasiemski designed the experiments. Céline Boidin-Wichlacz performed most of the experiments. Séphane Hourdez contributed to phylogenetic analyses. Ann Andersen contributed to the Transmission electron microscopy analysis. Céline Boidin-Wichlacz wrote the manuscript. Nathalie Jouy performed the research and analyzed the data in flow cytometry. Ann Andersen, Séphane Hourdez and Aurélie Tasiemski critically revised the manuscript.

Declarations of interest

The authors declare no potential conflicts of interests with respect to the research, authorship or publication of this article

Data Availability Statement

The dataset analyzed during the current study is available from the corresponding author on reasonable request.

Ethics approval

Not applicable

Acknowledgments

This work was funded by the FRB Region Hauts-de-France (VERMER project, 2014-2016), the Region Hauts-de-France (AniMo project, 2013), the University of Lille (BQR emergence), and the Total Foundation (PIONEER project, 2016-2018). The authors are grateful to Elisabeth Werkmeister of BioImaging Center Lille (UMS 2014-BICeL) for confocal microscopy. Virginie Cuvillier-Hot is acknowledged for fruitful discussions.

Table

Table 1. Sequence accession numbers for the phylogenetic approach.

Species	Protein	GenBank ID
Capitella teleta	Lysozyme	ELT93524
Hirudo medicinalis	Lysozyme i	AAA96144
Eisenia fetida	Lysozyme	AGJ83864
Eisenia andrei	Lysozyme	DQ339138
Mytilus edulis	Lysozyme i	ABB76765
Crassostrea virginica	Lysozyme i	BAE47520
Ruditapes philippinarum	Lysozyme i	BAC15553
Asterias rubens	Lysozyme i	AAR29291
Apostichopus japonicus	Lysozyme i	ABK34500
Bathymodiolus azoricus	Lysozyme i	AAN16208
Bathymodiolus thermophilus	Lysozyme i	AAN16209
Calyptogena sp.	Lysozyme i	AAN16211
Mytilus galloprovincialis	Lysozyme i	AJQ21515
	Lysozyme	OPL33781
Lamellibrachia satsuma	Lysozyme	KAI0215534
Dimorphilus gyrociliatus	DgyrCDS4060	CAD5115039
Urechis unicinctus	Invertebrate-type lysozyme	AWA82039
Platynereis dumerilii	Extracellular, globin Egb_A1a	QQO51916
	Globin Ngb	QQO51934
Arenicola marina	Haemoglobin B2	CAI56309
	Haemoglobin B1	CAJ32742
	Haemoglobin A2	CAI56308
	Haemoglobin A2b	CAJ32740
	Haemoglobin A2c	CAJ32741
Alvinella pompejana	Intracellular haemoglobin	Q53I62

Glycera dibranchiata	Extracellular globin	QAT81156
	Extracellular globin	QAT81157
	Extracellular globin	QAT81159
	Extracellular globin	QAT81158
	Globin P3	AAA29161
	Globin P2	AAA29160
	Globin P1	CAA37995
Lumbricus terrestris	Chain D, hemoglobin chain d1	56967019
	Extracellular, Chain B, Globin II	56967017
	Extracellular, Chain A, Globin IV	56967016
Lepidonotus semilectus	Extracellular, Chain C, Globin III,	56967018
	Extracellular globin	QAT81218
Halosydna brevisetosa	Extracellular globin	QAT81169
Aphrodita japonica	Neuroglobin	QKD76907
	Neuroglobin	QKD76908
Aphrodita aculeata	Nerve myoglobin	AAC47259
Branchipolynoe seepensis	Extracellular single-domain globin	ACU21605
Branchipolynoe symmytilida	Extracellular single-domain globin	ACU21604
	Extracellular tetra-domain globin	ACU21599
	Extracellular tetra-domain globin	ACU21598
	Extracellular tetra-domain globin	ACU21597
	Extracellular tetra-domain globin	ACU21596
Eulagiscinae sp.	Intracellular single-domain globin	ALH21945

Figures

Figure 1: **Coelomocyte population:** A) Flow cytometry analysis of *Capitella* C-Channel 1 cells. Gate 1 represents a homogeneous population of coelomocytes. The y-axis represents the dot plots of forward scatter-height (FSC-Height), versus side scatter-height (SSC-Height) on the x-axis. Each red dot represents a single cell that has passed through the instrument and debris are marked in gray. The yellow dots result from red dots overlapping each other. B) On whole-body longitudinal sections stained with toluidine blue, coelomocytes are visible inside the coelom throughout the middle part of the body. The red rectangle focuses on some of them in figure. C) Zoomed in view of the red rectangle in image B, showing that the coelomocytes appear of similar size and homogeneously stained around an eccentric nucleus. D) Microscopic observation of the natural red color of the coelomocytes, indicating they are erythrocytes. E) Observation of the smooth outer surface of the coelomocytes by scanning electron microscopy. Abbreviations: c. Cytoplasm, Cc. Coelomocyte, Cu. Cuticle, Dt. digestive tract, Lm. longitudinal muscles, n. nucleus.

Figure 2: **Cell description**. A) Staining of coelomocytes by labeling nuclear DNA with DAPI. Presence of a single dense body (arrow) in the cytoplasm. B) Electron microscopy images showing circulating cells. White arrows show electron dense bodies. C) Transmission electron microscopy of a circulating cell in the coelomic cavity. The black arrow shows a polyribosome. D) Neutral red stain

with emphasis on a bright pink-tinted alkaline structure (black arrow) and yellow/orange colored acidic vacuoles (white arrow). Abbreviations: c. cytoplasm, m. mitochondria, n. nucleus, v. vacuoles.

Figure 3: **Respiratory pigment**. A) Perls' stain was used to reveal iron stores. Iron deposit appears as a bright blue granular staining (black arrows) all around the periphery of the cytoplasm. B) Live whole body observed under binocular microscope showing the natural red color of coelomocytes. The white dotted lines delimit the setigerous segments. C) Detection of intracellular hemoglobin transcript by RT-PCR in coelomocytes. D) Spectral data of all cells in the mixture obtained under a 488 nm laser. E) Spectral data of all cells in the mixture obtained under 405 and 638nm laser excitation spectrum charts. The red arrow indicates the cells spectrum with a high content of hemoglobin. The black arrow indicates the cells spectrum with a low content of hemoglobin. Abbreviations: Cc. Coelomic cells, He. Hemoglobin, Dt. Digestive tract, M. DNA ladder (100 bp).
.

Figure 4 : The origin of the globin found in the coelomocytes of C-Channel1. Maximum likelihood phylogenetic tree of representatives of the typical intracellular or extracellular hemoglobins, as well as myoglobins (Mb), neuroglobins (Ngb), and the unusual polynoid extracellular hemoglobins. The tree was produced with PhyML based on an alignment of 51 proteins (192 amino acid positions) using a Dayhoff matrix. The nodes' confidence was evaluated with a bootstrap approach for 100 replicates (only values greater than 70 are indicated). Species names and accession numbers are indicated in the node labels. The blue rectangle shows the extracellular globin lineage, the orange rectangle indicates the unusual polynoid extracellular globins. All other globins are intracellular (neuroglobin, myoglobin, and erythrocytic gobins). The green rectangle indicates the known *Capitella teleta* (Cte) globins extracted from the genome, and this lineage includes the *Capitella* C-Channel 1 globin (large arrow). Lte= *Lumbricus terrestris*

Figure 5: **Phagocytic activity.** A) Light microphotograph of coelomocytes with toluidine blue-stained *Saccharomyces cerevisiae* (arrows point at Baker's yeast type II). B) Flow cytometry analysis to verify the labelling of bacteria mixed with a 50% ratio of *Vibrio alginolyticus* and *Bacillus hwajinpoensis.* The left column shows the Side Scatter Channel/FITC plot of non-stained bacteria i.e. their level of autofuorescence. The right column corresponds to Side Scatter /FITC plot of bacteria labeled with green fluorescence (FITC) showing their high level of fluorescence. In both figures, the box framed B corresponds to the positive region of labelled bacteria. C) The scatter plots for un-labelled Capitella cells: in left column, the FSC/ SSC plot and in the right column their FITC/ red emission plot. D) The scatter plots for Capitella cells in contact with FITC-labelled bacteria : in the left column the FSC/ SSC emission plot. On each figure, the red boxes frame the cells with low

hemoglobin level. These experiments were performed three times (n=3). E) Cellural phagocytosis analyzed by confocal microscopy. Cell samples were acquired in 3D using the Imaris software. The double staining allowed to clearly establish whether or not a green FITC-labeled bacteria was internalized by an erythrocyte stained in red with SYTO 60. F) Optical sections of the previous figure with orthogonal views, showing successively a single plane in the three directions; xy, xz or yz as indicated (by thewhite lines). This enabled to check the exact location of the green fluorescing bacteria within the red cytoplasm of cell. Scale bar for all panels is 3 μm.

Figure 6: **Antimicrobial protection.** A) Phylogenetic tree of lysozyme sequences from various invertebrate species. The tree was constructed with a maximum likelihood (ML) approach on a 79 amino-acid alignment. The Dayhoff matrix was used for substitutions. Values at nodes are bootstrap values out of 100 replicates (only values greater than 70 are shown). The sequences from the echinoderms *Apostichopus japonicus* and *Asterias rubens* were used as outgroups. The blue rectangle indicates annelid sequences and the sequence from C-Channel 1 is indicated by the black arrow. B) Lysozyme activity was measured using the *M. luteus* lytic assay on a 90 mm diameter gel-coated box. The diameter of the cleared zones is represented by a red dotted circle. Animal (a), coelomocytes (c), microbially challenged animals (ab), microbially challenged cells (cb). C) PCR-Expression of lysozymes in different fractions, whole animal (a), coelomocytes (c) and microbially challenged whole animal (ab) or cells (cb). PCR control (Co) and marker (M) corresponds to the DNA ladder (100 bp).

Figure 7: ***Cc*-Lumbricin and *Cc*-Capitellacin distribution**. A) RT-PCR using primers for GAPDH (GlycerAldehyde-3-Phosphate DeHydrogenase), *Cc*-Capitellacin and *Cc*-Lumbricin. Expression in different fractions, whole animal (a), coelomocytes (c) and microbially challenged whole animal (ab) or cells (cb). GAPDH was used as constitutive control. Marker (M) represents a 100 bp DNA ladder is shown on the left and the PCR negative control with primers is indicated (CN). B) Western blot analysis of peptide extracts with anti-Lumbricin. The framed box highlights a slight peptide band with a molecular weight between 4.3 and 10 kDa present in the mucus of *Capitella*, but not in the whole animal. C) Western blot analysis of peptide extracts with anti-Capitellacin. The framed box highlights the presence of a massive band of peptides sizing between 4.6 and 10 kDa in the whole animal, particularly when bacterially challenged, but not detectable within its mucus. D) SDS-polyacrylamide gel of Coomassie blue-stained fractions. Animal (a), the microbially challenged whole animal (ab), mucus (m), mucus of microbially challenged animal (mb).

Figure 8: **Localization of *Cc*-Lumbricin and *Cc*-Capitellacin in *Capitella* C-Channel 1, after bacterial challenge with *V. alginolytcu*s and *Bacillus hwajinpoensis.*** *Cc*-Lumbricin was labeled by anti-*Hm*-Lumbricin and Alexa 488 (green) in figures A to E. *Cc*-Capitellacin was labeled by anti-Capitellacin and Alexa 488 (green) in figures F to H. DNA was labeled by DAPI stain (blue) and

merged images are shown with ZEISS Axio Imager 2. A) Longitudinal body section of a C-Channel 1 control. B) Section of C-Channel1 stimulated by bacteria for 16 hours. C) Controls, performed with pre-immune serum. A1-B1-C1) Zoomed in section of the integument from the previous image. D) Anti-Lumbricin antibody green labeling of bacteria trapped inside the mucus of *Capitella* stimulated with bacteria. E) Pre-immune labeling of bacteria trapped inside the mucus of C-Channel1 stimulated bacteria. F) Transversal section of a C-Channel1 control. G) Section of C-Channel1 stimulated by bacteria for 16 hours. H) Controls performed with pre-immune serum. F1-G1-H1) Zoomed in section of the integument from the previous image. Abbreviations: Cc. coelomocyte, Co. coelom, Cu. Cuticle, Dt. digestive tract, e. epidermis.

References

Abele-Oeschger, D., Oeschger, R., 1995. Hypoxia-induced autoxidation of haemoglobin in the benthic invertebrates *Arenicola marina* (Polychaeta) and *Astarte borealis* (Bivalvia) and the possible effects of sulphide. J. Exp. Mar. Bio. Ecol. 187, 63–80. https://doi.org/10.1016/0022-0981(94)00172-A

Bailly, X., Vinogradov, S., 2005. The sulfide binding function of annelid hemoglobins: Relic of an old biosystem? J. Inorg. Biochem. 99, 142–150. https://doi.org/10.1016/j.jinorgbio.2004.10.012

Bao, Y., Wang, J., Li, C., Li, P., Wang, S., Lin, Z., 2016. A preliminary study on the antibacterial mechanism of *Tegillarca granosa* hemoglobin by derived peptides and peroxidase activity. Fish Shellfish Immunol. 51, 9–16. https://doi.org/10.1016/j.fsi.2016.02.004

Baskin, D., 1974. The coelomocytes of nereid polychaetes, in: Contemporary Topics In Immunobiology Volume 4 Invertebrate Immunology. pp. 55–64. https://doi.org/10.1007/978-1-4684-3048-6

Belato, F.A., Coates, C.J., Halanych, K.M., Weber, R.E., Costa-Paiva, E.M., 2020. Evolutionary history of the globin gene family in annelids. Genome Biol. Evol. 12, 1719–1733. https://doi.org/10.1093/GBE/EVAA134

Berlov, M., Maltseva, A., 2016. Immunity of the lugworm *Arenicola marina*: cells and molecules. Invertebr. Surviv. J. 13, 247–256.

Bleidorn, C., Vogt, L., Bartolomaeus, T., 2003. New insights into polychaete phylogeny (Annelida) inferred from 18S rDNA sequences. Mol. Phylogenet. Evol. 29, 279–288. https://doi.org/10.1016/S1055-7903(03)00107-6

Bodó, K., Boros, Á., Rumpler, É., Molnár, L., Böröcz, K., Németh, P., Engelmann, P., 2019. Identification of novel lumbricin homologues in *Eisenia andrei* earthworms. Dev. Comp.

802 Immunol. 90, 41–46. https://doi.org/10.1016/j.dci.2018.09.001

803 Boidin-Wichlacz, C., Jollivet, D., Papot, C., Roisin, L., Massol, F., Tasiemski, A., 2021. Genetic
804 diversification and life-cycle of the polychaete *Capitella* spp. from the English Channel:
805 evidence for sympatric cryptic species and alternative reproductive strategies. Mar. Biol. 168.
806 https://doi.org/10.1007/s00227-021-03972-2

807 Boidin-Wichlacz, C., Vergote, D., Slomianny, C., Jouy, N., Salzet, M., Tasiemski, A., 2012.
808 Morphological and functional characterization of leech circulating blood cells: role in immunity
809 and neural repair. Cell. Mol. Life Sci. 69, 1717–1731.

810 Boyle, M.J., Yamaguchi, E., Seaver, E.C., 2014. Molecular conservation of metazoan gut formation:
811 Evidence from expression of endomesoderm genes in *Capitella teleta* (Annelida). Evodevo 5, 1–
812 19. https://doi.org/10.1186/2041-9139-5-39

813 Bruno, R., Maresca, M., Canaan, S., Cavalier, J.-F., Mabrouk, K., Boidin-Wichlacz, C., Olleik, H.,
814 Zeppilli, D., Brodin, P., Massol, F., Jollivet, D., Jung, S., Tasiemski, A., 2019. Worms'
815 antimicrobial peptides. Mar. Drugs 17. https://doi.org/10.3390/md17090512

816 Cho, J.H., Park, C.B., Yoon, Y.G., Kim, S.C., 1998. Lumbricin I, a novel proline-rich antimicrobial
817 peptide from the earthworm: Purification, cDNA cloning and molecular characterization.
818 Biochim. Biophys. Acta - Mol. Basis Dis. 1408, 67–76. https://doi.org/10.1016/S0925-
819 4439(98)00058-1

820 Coates, C.J., Decker, H., 2016. Immunological properties of oxygen-transport proteins: hemoglobin,
821 hemocyanin and hemerythrin. Cell. Mol. Life Sci. 74, 293–317. https://doi.org/10.1007/s00018-
822 016-2326-7

823 Cuvillier-Hot, V., Boidin-Wichlacz, C., Tasiemski, A., 2014. Polychaetes as annelid models to study
824 ecoimmunology of marine organisms. J. Mar. Sci. Technol. 22. https://doi.org/10.6119/JMST-
825 013-0718-1

826 Cuvillier-Hot, V., Gaudron, S.M., Massol, F., Boidin-Wichlacz, C., Pennel, T., Lesven, L., Net, S.,
827 Papot, C., Ravaux, J., Vekemans, X., Billon, G., Tasiemski, A., 2018. Immune failure reveals
828 vulnerability of populations exposed to pollution in the bioindicator species *Hediste*
829 *diversicolor*. Sci. Total Environ. 613–614. https://doi.org/10.1016/j.scitotenv.2017.08.259

830 Dales, P.R., 1964. The coelomocytes of the terebellid polychaete *Amphitrite johnstoni*. J. Cell Sci. s3-
831 105, 263–279.

832 Davidson, C.R., Best, N.M., Francis, J.W., Cooper, E.L., Charles, T., 2008. Toll-like receptor genes (
833 TLRs) from *Capitella capitata* and *Helobdella robusta* (Annelida) 608–612.
834 https://doi.org/10.1016/j.dci.2007.11.004

Dhainaut, A., Porchet-Henneré, E., 1988. Haemocytes and coelomocytes. The Ultrastructure of Polychaeta Microfauna Marina., in: Westheide, W., Hermans, C.. (Eds.), Gustav Fischer Verlag. pp. 215–230.

Diaz, R.J., Rosenberg, R., 1995. Marine benthic hypoxia: a review of its ecological effects and the behavioural responses of benthic macrofauna. Oceanogr. Mar. Biol. an Annu. Rev. Vol. 33 245–303.

Fischer, A., Hoeger, U., 1993. Metabolic links between somatic sexual maturation and oogenesis in nereid annelids—a brief review. Invertebr. Reprod. Dev. 23, 131–138. https://doi.org/https://doi.org/10.1080/07924259.1993.9672304

Fontaine, A.R., Hall, B.D., 1981. The haemocyte of the holothurian *Eupentacta quinquesemita*: ultrastructure and maturation. Can. J. Zool. 59, 1884–1891. https://doi.org/https://doi.org/10.1139/z81-256

Fontaine, A.R., Lambert, P., 1977. The fine structure of the leucocytes of the holothurian, *Cucumaria miniata*. Can. J. Zool. 55, 77–198. https://doi.org/https://doi.org/10.1139/z77-198

Franchini, A., Simonini, R., Ottaviani, E., 2016. Coelomic cells of the marine fireworm *Hermodice carunculata* (Annelida , Polychaeta). Inv. Surv. J 13, 18–22. https://doi.org/https://doi.org/10.25431/1824-307X/isj.v13i1.18-22

Glomski, C.A., Tamburlin, J., 1990. The phylogenetic odyssey of the erythrocyte. II. The early or invertebrate prototypes. Histol. Histopathol. 5, 513–525.

Goodrich, E.S., 1898. Memoirs: On the Nephridia of the Polychæta. J. Cell Sci. s2-41, 439–457. https://doi.org/10.1242/jcs.s2-41.163.439

Grossmann, S., Reichardt, W., 1991. Impact of *Arenicola marina* on bacteria in intertidal sediments. Mar. Ecol. Prog. Ser. 77, 85–93. https://doi.org/10.3354/meps077085

Hourdez, S., Boidin-Wichlacz, C., Jollivet, D., Massol, F., Rayol, M.C., Bruno, R., Zeppilli, D., Thomas, F., Lesven, L., Billon, G., Duperron, S., Tasiemski, A., 2021. Investigation of *Capitella* spp. symbionts in the context of varying anthropic pressures: First occurrence of a transient advantageous epibiosis with the giant bacteria Thiomargarita sp. to survive seasonal increases of sulfides in sediments. Sci. Total Environ. 798. https://doi.org/10.1016/j.scitotenv.2021.149149

Hourdez, S., Lallier, F.H., De Cian, M.C., Green, B.N., Weber, R.E., Toulmond, A., 2000. Gas transfer system in *Alvinella pompejana* (Annelida polychaeta, Terebellida): functional properties of intracellular and extracellular hemoglobins. Physiol. Biochem. Zool. 73, 365–373. https://doi.org/10.1086/316755

867 Hourdez, S., Lallier, F.H., Martin-Jézéquel, V., Weber, R.E., Toulmond, A., 1999. Characterization
868 and functional properties of the extracellular coelomic hemoglobins from the deep-sea,
869 hydrothermal vent scaleworm *Branchipolynoe symmytilida*. Proteins Struct. Funct. Genet. 34,
870 435–442. https://doi.org/10.1002/(SICI)1097-0134(19990301)34:4<435::AID-
871 PROT3>3.0.CO;2-H

872 Jouin-Toulmond, C., Augustin, D., Toulmond, A., 1996. The gas transfert system in alvinellids
873 (annelida Polychaeta, Terebellida). Anatomy and ultrastructure of the anterior circulatory system
874 and characterization of coelomic, intracellular, haemoglobin. Cah. Biol. Mar. 37, 135.
875 https://doi.org/10.1002/adma.200900375

876 Kobayashi, G., Itoh, H., Nakajima, N., 2022. First mitochondrial genomes of Capitellidae and
877 Opheliidae (Annelida) and their phylogenetic placement. Mitochondrial DNA Part B Resour. 7,
878 577–579. https://doi.org/10.1080/23802359.2022.2056537

879 Li, W., Li, S., Zhong, J., Zhu, Z., Liu, J., Wang, W., 2011. A novel antimicrobial peptide from skin
880 secretions of the earthworm, *Pheretima guillelmi* (Michaelsen). Peptides. 32, 1146–50.
881 https://doi.org/10.1016/j.peptides.2011.04.015

882 Liebmann, E., 1942. The role of the chloragogue in regeneration of *Eisenia foetida* (Sav). J. Mophol.
883 70, 151–187. https://doi.org/https://doi.org/10.1002/jmor.1050700202

884 Maltseva, A.L., Kotenko, O.N., Kokryakov, V.N., Starunov, V. V., Krasnodembskaya, A.D., 2014.
885 Expression pattern of arenicin the antimicrobial peptides of polychaete *Arenicola marina*. Front.
886 Physiol. 5, 1–11. https://doi.org/10.3389/fphys.2014.00497

887 Mangum, C.P., Colacino, J.M., Grassle, J.P., 1992. Red Blood Cell Oxygen Binding in Capitellid
888 Polychaetes. Biol. Bull. 182, 129–134. https://doi.org/10.2307/1542187

889 Meyer, C., André, T., Purschke, G., 2021. Ultrastructure and functional morphology of the appendages
890 in the reef-building sedentary polychaete *Sabellaria alveolata* (Annelida, Sedentaria, Sabellida).
891 BMC Zool. 6, 1–25. https://doi.org/10.1186/s40850-021-00068-8

892 Osserman, E.F., Lawlor, D.P., 1966. Serum and urinary lysozyme (muramidase) in monocytic and
893 monomyelocytic leukemia. J.ExpMed 124, 921–952. https://doi.org/10.1084/jem.124.5.921

894 Ovchinnikova, T. V., Aleshina, G.M., Balandin, S. V., Krasnosdembskaya, A.D., Markelov, M.L.,
895 Frolova, E.I., Leonova, Y.F., Tagaev, A. a., Krasnodembsky, E.G., Kokryakov, V.N., 2004.
896 Purification and primary structure of two isoforms of arenicin, a novel antimicrobial peptide
897 from marine polychaeta *Arenicola marina*. FEBS Lett. 577, 209–214.
898 https://doi.org/10.1016/j.febslet.2004.10.012

899 Persinina, M., Chaga, O., 1994. Renewal and differentiation of the coelomic fluid cells of

thepolychaete *Arenicola marina*. I: Morphology andclassification of coelomocytes. Tsitogiia 36, 261–267.

Porchet-Henneré, E., Vernet, G., 1992. Cellular immunity in an annelid (*Nereis diversicolor*, Polychaeta): Production of melanin by a subpopulation of granulocytes. Cell Tissue Res. 269, 167–174. https://doi.org/10.1007/BF00384737

Projecto-Garcia, J., Le Port, A.S., Govindji, T., Jollivet, D., Schaeffer, S.W., Hourdez, S., 2017. Evolution of Single-Domain Globins in Hydrothermal Vent Scale-Worms. J. Mol. Evol. 85, 172–187. https://doi.org/10.1007/s00239-017-9815-7

Ravaux, J., Hamel, G., Zbinden, M., Tasiemski, A.A., Boutet, I., Léger, N., Tanguy, A., Jollivet, D., Shillito, B., 2013. Thermal Limit for Metazoan Life in Question: In Vivo Heat Tolerance of the Pompeii Worm. PLoS One 8, 4–9. https://doi.org/10.1371/journal.pone.0064074

Reish, D., Gerlinger, T., 1997. A review of the toxicological studies with polychaetous annelids. Bull. Mar. Sci. 60, 584–607.

Safronova, V.N., Panteleev, P. V., Sukhanov, S. V., Toropygin, I.Y., Bolosov, I.A., Ovchinnikova, T. V., 2022. Mechanism of Action and Therapeutic Potential of the β-Hairpin Antimicrobial Peptide Capitellacin from the Marine Polychaeta *Capitella teleta*. Mar. Drugs 20. https://doi.org/10.3390/md20030167

Schikorski, D., Cuvillier-Hot, V., Leippe, M., Boidin-Wichlacz, C., Slomianny, C., Macagno, E., Salzet, M., Tasiemski, A., 2008. Microbial Challenge Promotes the Regenerative Process of the Injured Central Nervous System of the Medicinal Leech by Inducing the Synthesis of Antimicrobial Peptides in Neurons and Microglia. J. Immunol. 181, 1083–1095. https://doi.org/10.4049/jimmunol.181.2.1083

Seamonds, B., Forster, R.E., Gottlieb, A.J., 1971. Heterogeneity of the hemoglobin from the common bloodworm *Glycera dibranchiata*. J. Biol. Chem. 246, 1700–1705. https://doi.org/10.1016/s0021-9258(18)62367-1

Seamonds, B., Schumacher, H.R., 1972. Fine Structure of Erythrocytes of the Common Bloodworm *Glycera dibranchiata*. Cytologia (Tokyo). 37, 359–363. https://doi.org/https://doi.org/10.1508/cytologia.37.359

Seaver, E.C., 2016. Annelid models I: *Capitella teleta*. Curr. Opin. Genet. Dev. 39, 35–41. https://doi.org/10.1016/j.gde.2016.05.025

Seaver, E.C., Kaneshige, L.M., 2006. Expression of "segmentation" genes during larval and juvenile development in the polychaetes *Capitella* sp. I and *H. elegans*. Dev. Biol. 289, 179–194. https://doi.org/10.1016/j.ydbio.2005.10.025

933 Silva, C.F., Shimabukuro, M., Alfaro-lucas, J.M., Fujiwara, Y., Sumida, P.Y.G., Amaral, A.C.Z.,
934 2016. A new Capitella polychaete worm (Annelida : Capitellidae) living inside whale bones in
935 the abyssal South Atlantic. Deep. Res. Part I 108, 23–31.
936 https://doi.org/10.1016/j.dsr.2015.12.004

937 Song, S., Starunov, V., Bailly, X., Ruta, C., Kerner, P., Cornelissen, A.J.M., Balavoine, G., 2020.
938 Globins in the marine annelid *Platynereis dumerilii* shed new light on hemoglobin evolution in
939 bilaterians. BMC Evol. Biol. 20, 1–23. https://doi.org/10.1186/s12862-020-01714-4

940 Stanovova, M., 2019. Cells of the body cavity of annelids: Morphology, cytogenesis, functions.
941 Invertebr. Zool. 16, 254–282. https://doi.org/10.15298/invertzool. 16.3.03

942 Tasiemski, A., Jung, S., Boidin-Wichlacz, C., Jollivet, D., Cuvillier-Hot, V., Pradillon, F., Vetriani, C.,
943 Hecht, O., Sönnichsen, F.D., Gelhaus, C., Hung, C.-W., Tholey, A., Leippe, M., Grötzinger, J.,
944 Gaill, F., 2014. Characterization and function of the first antibiotic isolated from a vent
945 organism: The extremophile metazoan *Alvinella pompejana*. PLoS One 9.
946 https://doi.org/10.1371/journal.pone.0095737

947 Tasiemski, A., Schikorski, D., Le Marrec-Croq, F., Pontoire-Van Camp, C., Boidin-Wichlacz, C.,
948 Sautière, P.E., 2007. Hedistin: A novel antimicrobial peptide containing bromotryptophan
949 constitutively expressed in the NK cells-like of the marine annelid, *Nereis diversicolor*. Dev.
950 Comp. Immunol. 31, 749–762. https://doi.org/10.1016/j.dci.2006.11.003

951 Tasiemski, A., Vandenbulcke, F., Mitta, G., Lemoine, J., Lefebvre, C., Sautière, P.E., Salzet, M.,
952 2004. Molecular characterization of two novel antibacterial peptides inducible upon bacterial
953 challenge in an annelid, the leech *Theromyzon tessulatum*. J. Biol. Chem. 279, 30973–30982.
954 https://doi.org/10.1074/jbc.M312156200

955 Terwilliger, N.B., 1998. Functional adaptations of oxygen-transport proteins. J. Exp. Biol. 201, 1085–
956 1098. https://doi.org/10.1242/jeb.201.8.1085

957 Terwilliger, N.B., Terwilliger, R.C., Schabtach, E., 1985. Intracellular respiratory proteins of
958 Sipuncula, Echiura, and Annelida, in: Cohen, W.D. (Ed.), Blood Cells of Marine Invertebrates :
959 Experimental Systems in Cell Biology and Comparative Physiology. Alan R.Liss, New York, pp.
960 193–225.

961 Urakawa, H., Rivera, I.N.G., 2006. The biology of vibrios, in: Fabiano L. Thompson, Brian Austin,
962 J.S. (Ed.), Aquatic Environment. pp. 173–189. https://doi.org/10.1128/9781555815714

963 Vetvicka, V., Sima, P., 2009. Origins and functions of annelide immune cells : the concise survey.
964 Invertebr. Surviv. J. 6, 138–143.

965 Wang, Xin, Wang, Xiaoxu, Zhang, Y., Qu, X., Yang, S., 2003. An antimicrobial peptide of the

966 earthworm *Pheretima tschiliensis*: cDNA cloning, expression and immunolocalization.
967 Biotechnol. Lett. 25, 1317–1323. https://doi.org/10.1023/A:1024999206117

968 Weber, R.E., Vinogradov, S.N., 2001. Nonvertebrate hemoglobins: Functions and molecular
969 adaptations. Physiol. Rev. 81, 569–628. https://doi.org/10.1152/physrev.2001.81.2.569

970 Weidong, P., Xianghui, L., Feng, G., Jie, H., Tao, Z., 2003. a Novel Antimicrobial Clamworm
971 *Perinereis aibuhitensis* Characterization Peptide Grube Purified from and Its Partial the This
972 novel named Test Microbes-Seven. J.Biochem 135, 297–304.
973 https://doi.org/https://doi.org/10.1093/jb/mvh036

974 Wells, R.M.G., Warren, L.M., 1975. The function of the cellular haemoglobins in *Capitella capitata*
975 (Fabricius) and *Notomastus latericeus* Sars (Capitellidae: Polychaeta). Comp. Biochem. Physiol.
976 -- Part A Physiol. 51, 737–740. https://doi.org/10.1016/0300-9629(75)90048-1

977 Wippler, J., Kleiner, M., Lott, C., Gruhl, A., Abraham, P.E., Giannone, R.J., Young, J.C., Hettich,
978 R.L., Dubilier, N., 2016. Transcriptomic and proteomic insights into innate immunity and
979 adaptations to a symbiotic lifestyle in the gutless marine worm *Olavius algarvensis*. BMC
980 Genomics 17, 1–19. https://doi.org/10.1186/s12864-016-3293-y

981 Wu, R., Patocka, J., Nepovimova, E., Oleksak, P., Valis, M., Wu, W., Kuca, K., 2021. Marine
982 Invertebrate Peptides: Antimicrobial Peptides. Front. Microbiol. 12, 1–12.
983 https://doi.org/10.3389/fmicb.2021.785085

984 Zal, F., Leize, E., Lallier, F.H., Toulmond, A., Van Dorsselaer, A., Childress, J.J., 1998. S-
985 sulfohemoglobin and disulfide exchange: The mechanisms of sulfide binding by *Riftia*
986 *pachyptila* hemoglobins. Proc. Natl. Acad. Sci. U. S. A. 95, 8997–9002.
987 https://doi.org/10.1073/pnas.95.15.8997

988 Zavalova, L.L., Antipova, N. V., Fadeeva, Y.I., Pavlyukov, M.S., Pletneva, N. V., Pletnev, V.Z.,
989 Baskova, I.P., 2012. Catalytic sites of medicinal leech enzyme destabilase-lysozyme (mlDL):
990 Structure-function relationship. Russ. J. Bioorganic Chem. 38, 198–202.
991 https://doi.org/10.1134/S1068162012020148

992

Figure 1

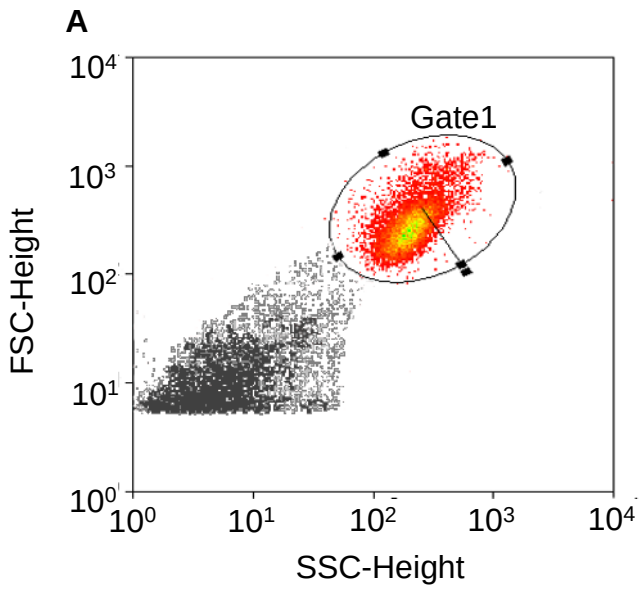
A
Gate1
FSC-Height
SSC-Height
10^0
10^1
10^2
10^3
10^4

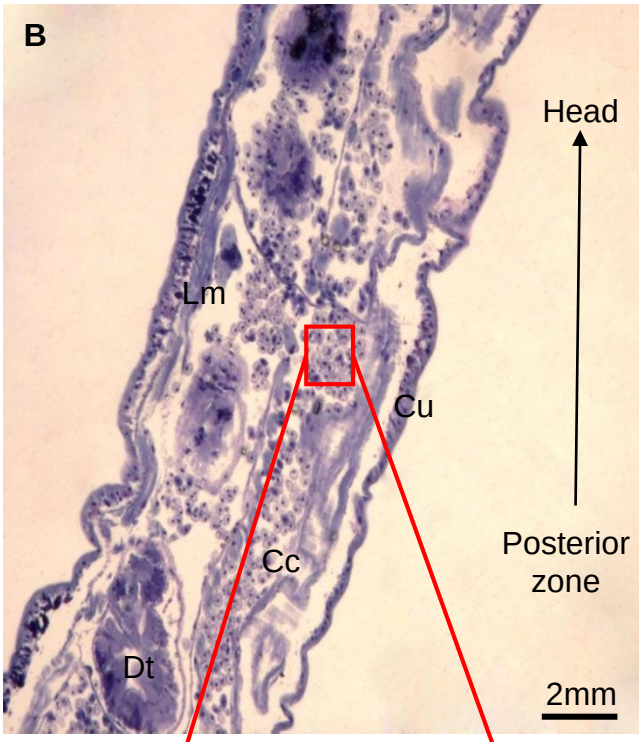
B
Head
Lm
Cu
Cc
Dt
Posterior zone
2mm


D
10µm

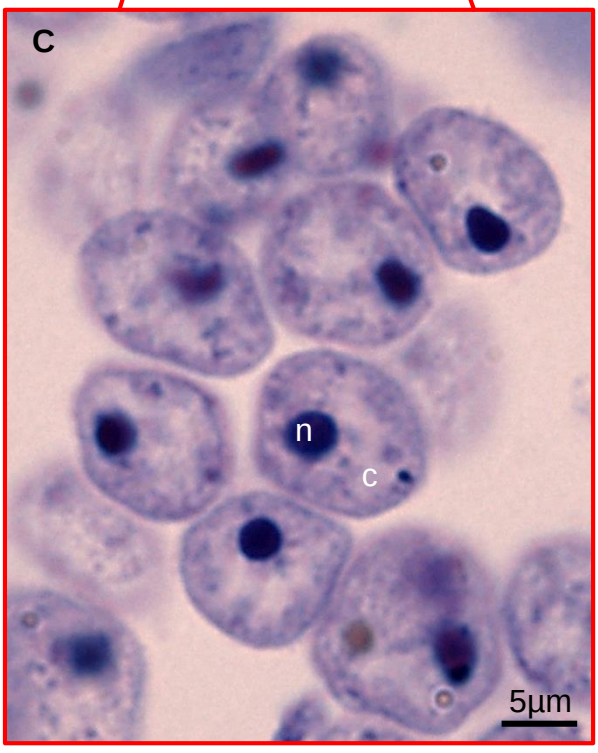
C
n
c
5µm

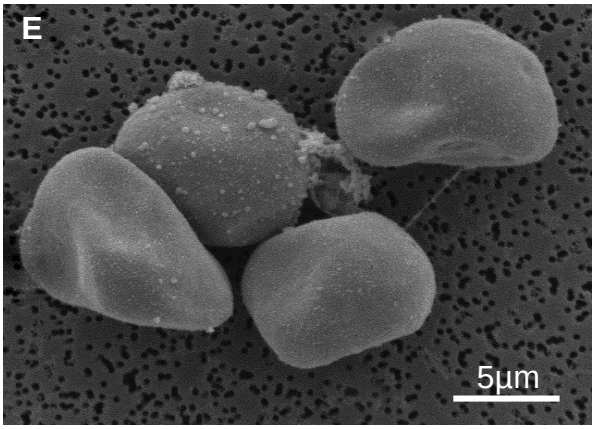
E
5µm

Figure 2

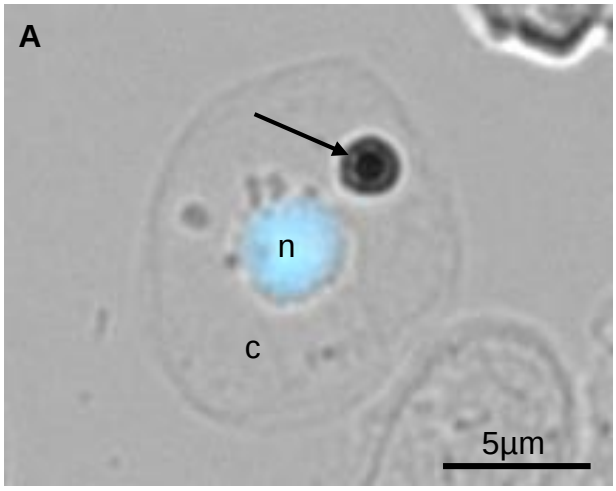

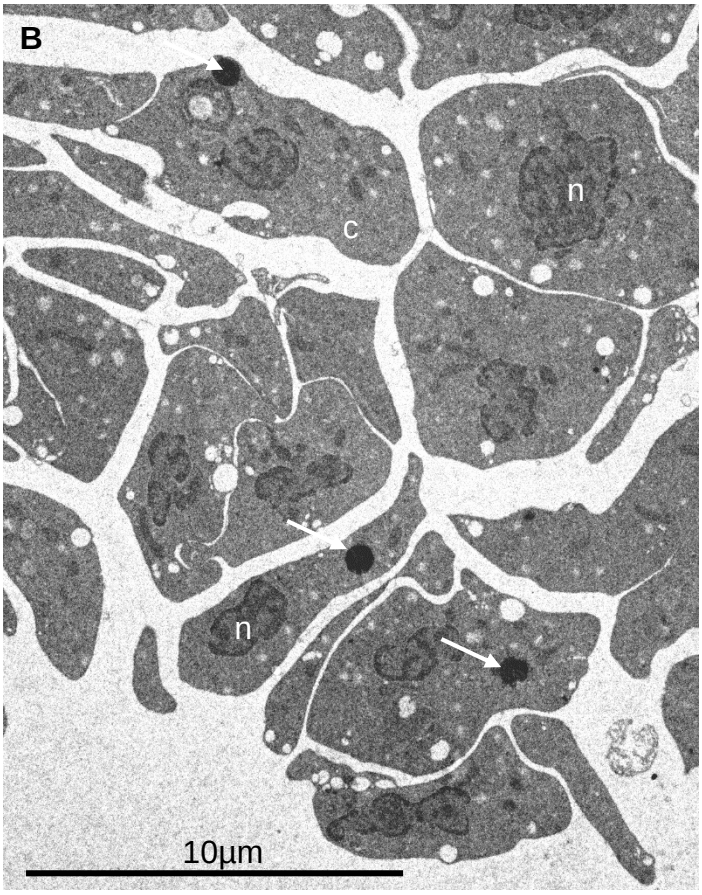

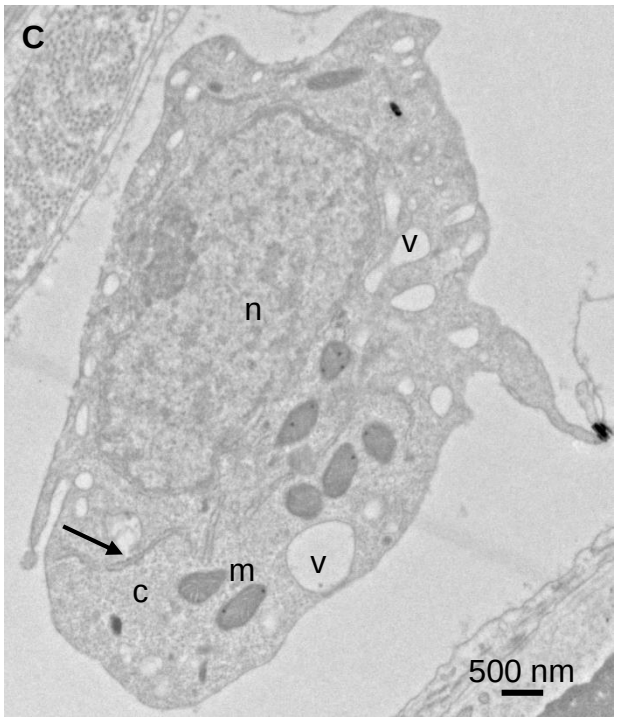

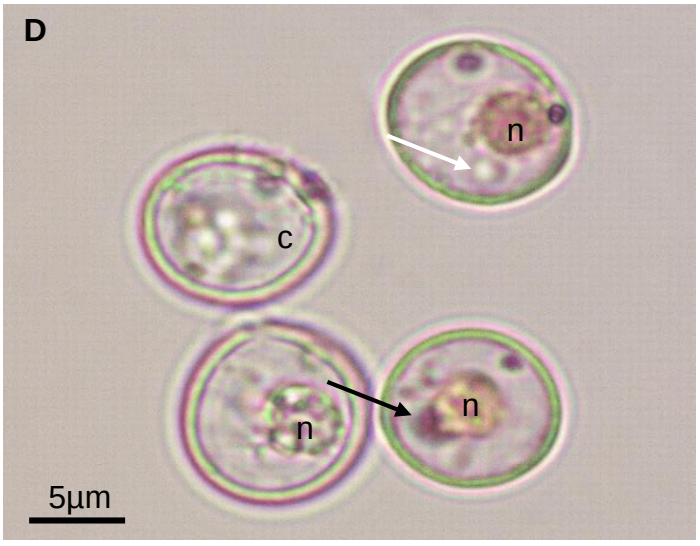

Figure 3

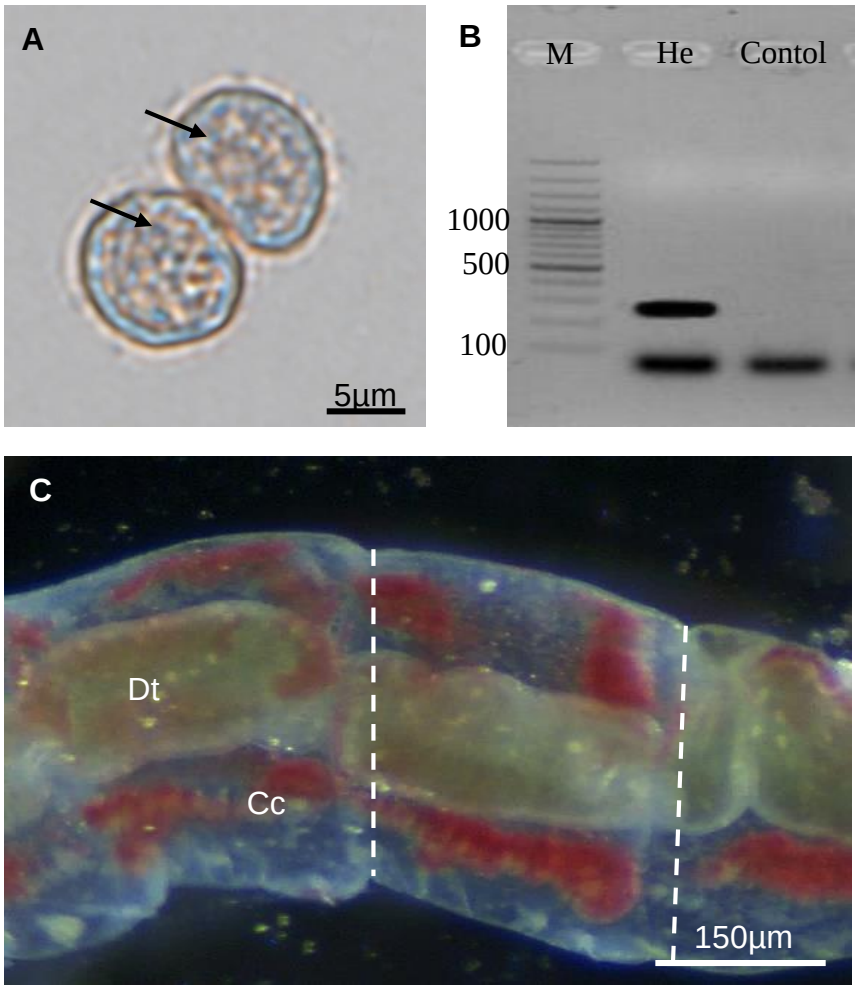
A
5μm
B
M
He
Contol
1000
500
100
C
Dt
Cc
150μm
D
LD488_H
Wavelength
E
LD405/638_H
Wavelength

Figure 4

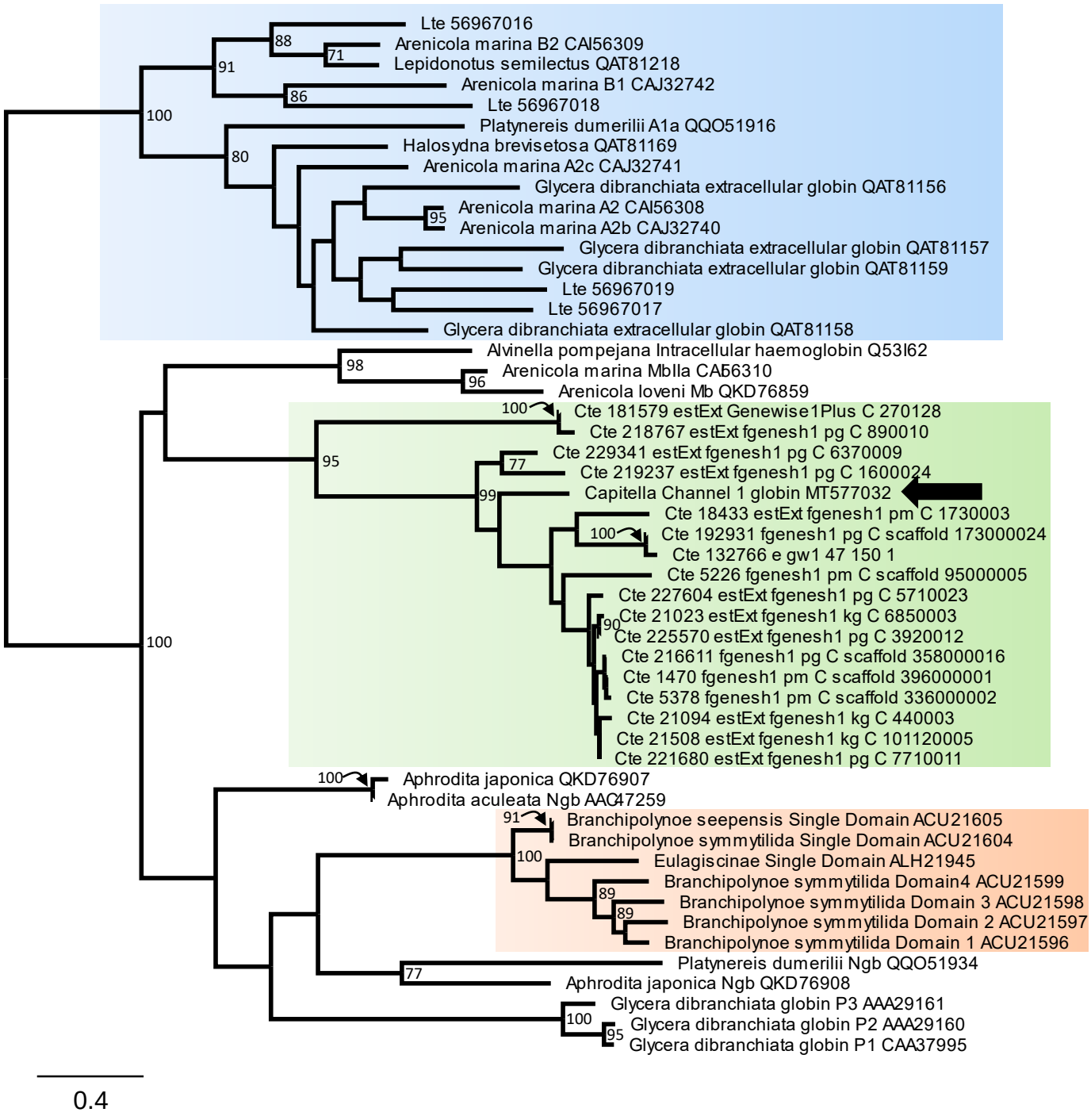
Lte 56967016
Arenicola marina B2 CAI56309
Lepidonotus semilectus QAT81218
Arenicola marina B1 CAJ32742
Lte 56967018
Platynereis dumerilii A1a QQO51916
Halosydna brevisetosa QAT81169
Arenicola marina A2c CAJ32741
Glycera dibranchiata extracellular globin QAT81156
Arenicola marina A2 CAI56308
Arenicola marina A2b CAJ32740
Glycera dibranchiata extracellular globin QAT81157
Glycera dibranchiata extracellular globin QAT81159
Lte 56967019
Lte 56967017
Glycera dibranchiata extracellular globin QAT81158
Alvinella pompejana Intracellular haemoglobin Q53I62
Arenicola marina MbIIa CA56310
Arenicola loveni Mb QKD76859
Cte 181579 estExt Genewise1Plus C 270128
Cte 218767 estExt fgenesh1 pg C 890010
Cte 229341 estExt fgenesh1 pg C 6370009
Cte 219237 estExt fgenesh1 pg C 1600024
Capitella Channel 1 globin MT577032
Cte 18433 estExt fgenesh1 pm C 1730003
Cte 192931 fgenesh1 pg C scaffold 173000024
Cte 132766 e gw1 47 150 1
Cte 5226 fgenesh1 pm C scaffold 95000005
Cte 227604 estExt fgenesh1 pg C 5710023
Cte 21023 estExt fgenesh1 kg C 6850003
Cte 225570 estExt fgenesh1 pg C 3920012
Cte 216611 fgenesh1 pg C scaffold 358000016
Cte 1470 fgenesh1 pm C scaffold 396000001
Cte 5378 fgenesh1 pm C scaffold 336000002
Cte 21094 estExt fgenesh1 kg C 440003
Cte 21508 estExt fgenesh1 kg C 101120005
Cte 221680 estExt fgenesh1 pg C 7710011
Aphrodita japonica QKD76907
Aphrodita aculeata Ngb AAC47259
Branchipolynoe seepensis Single Domain ACU21605
Branchipolynoe symmytilida Single Domain ACU21604
Eulagiscinae Single Domain ALH21945
Branchipolynoe symmytilida Domain4 ACU21599
Branchipolynoe symmytilida Domain 3 ACU21598
Branchipolynoe symmytilida Domain 2 ACU21597
Branchipolynoe symmytilida Domain 1 ACU21596
Platynereis dumerilii Ngb QQO51934
Aphrodita japonica Ngb QKD76908
Glycera dibranchiata globin P3 AAA29161
Glycera dibranchiata globin P2 AAA29160
Glycera dibranchiata globin P1 CAA37995
0.4

Figure 5

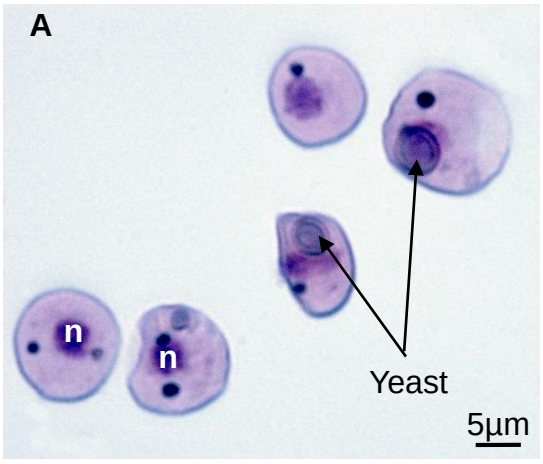

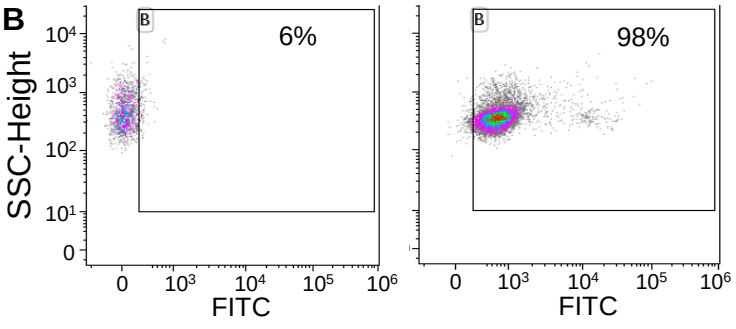

Gate	% Gated
All	100.00
B	6.93

Gate	% Gated
All	100.00
B	98.41

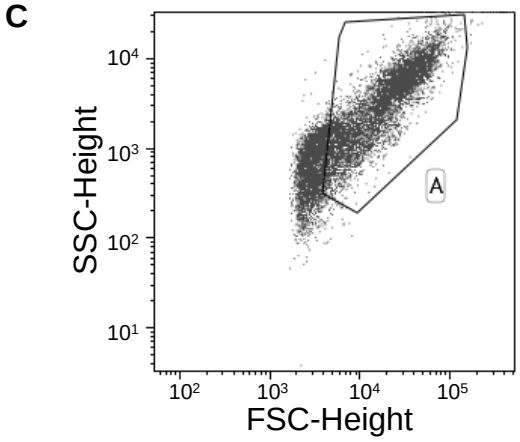

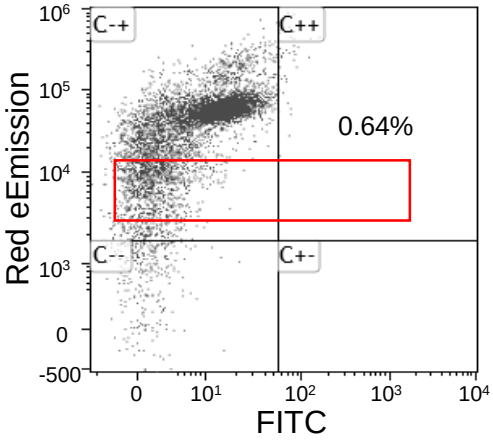

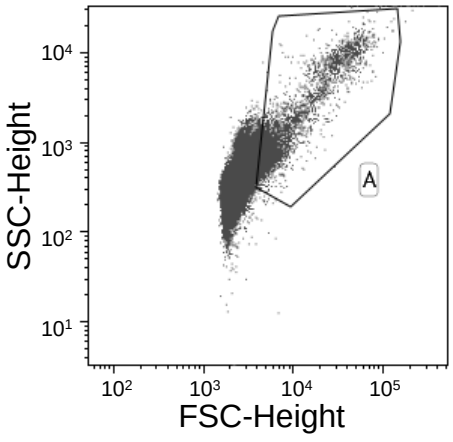

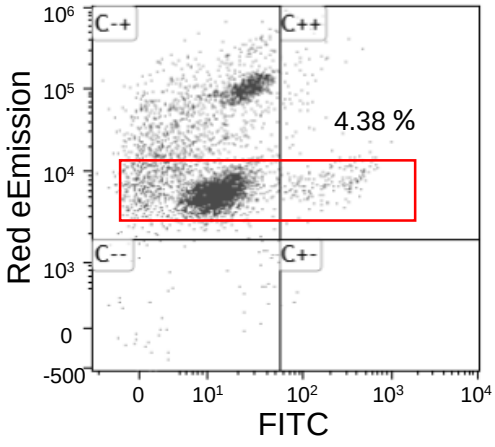

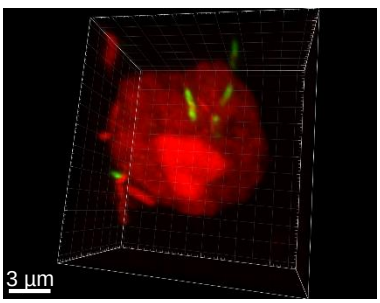

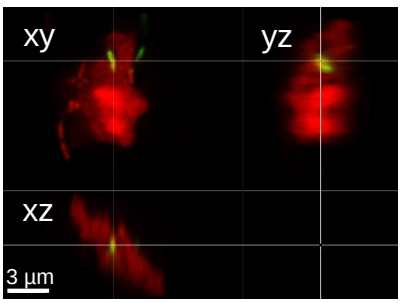

Figure 6

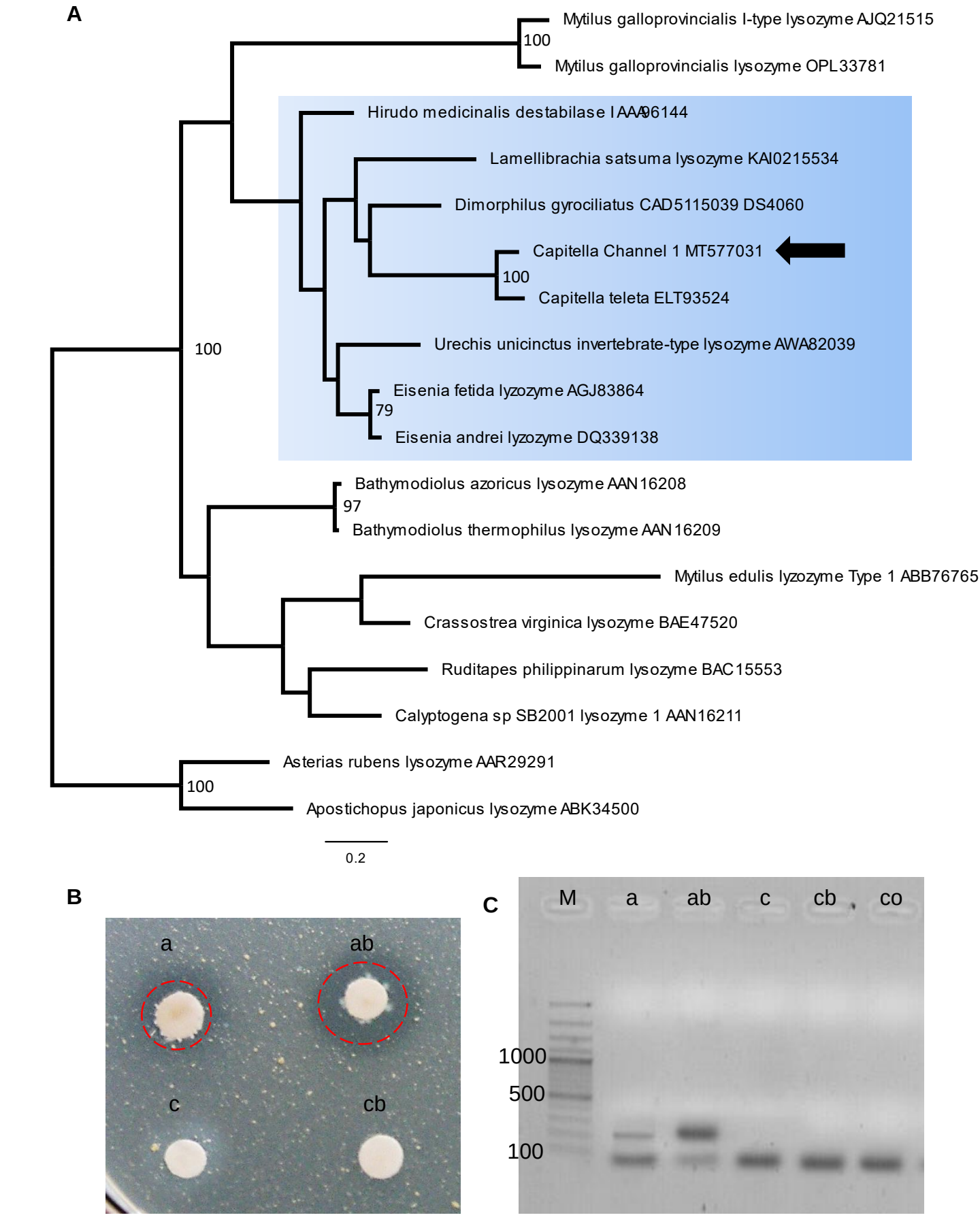
A
Mytilus galloprovincialis I-type lysozyme AJQ21515
100
Mytilus galloprovincialis lysozyme OPL33781
Hirudo medicinalis destabilase IAAA96144
Lamellibrachia satsuma lysozyme KAI0215534
Dimorphilus gyrociliatus CAD5115039 DS4060
Capitella Channel 1 MT577031
100
Capitella teleta ELT93524
100
Urechis unicinctus invertebrate-type lysozyme AWA82039
Eisenia fetida lyzozyme AGJ83864
79
Eisenia andrei lyzozyme DQ339138
Bathymodiolus azoricus lysozyme AAN16208
97
Bathymodiolus thermophilus lysozyme AAN16209
Mytilus edulis lyzozyme Type 1 ABB76765
Crassostrea virginica lysozyme BAE47520
Ruditapes philippinarum lysozyme BAC15553
Calyptogena sp SB2001 lysozyme 1 AAN16211
Asterias rubens lysozyme AAR29291
100
Apostichopus japonicus lysozyme ABK34500
0.2
B
a
ab
c
cb
C
M
a
ab
c
cb
co
1000
500
100

Figure 7

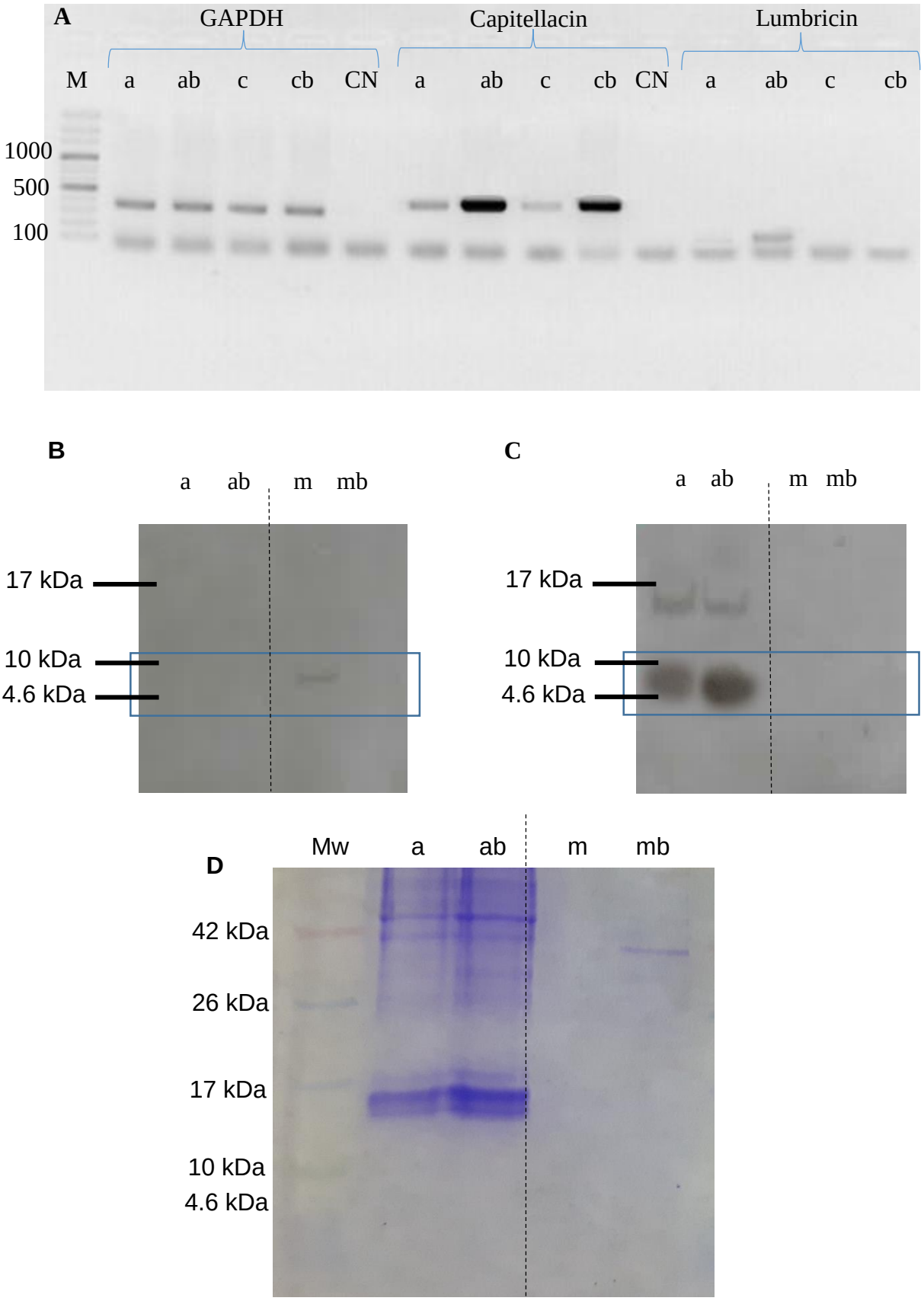
A
GAPDH
Capitellacin
Lumbricin
M
a
ab
c
cb
CN
a
ab
c
cb
CN
a
ab
c
cb
1000
500
100
B
a
ab
m
mb
17 kDa
10 kDa
4.6 kDa
C
a
ab
m
mb
17 kDa
10 kDa
4.6 kDa
D
Mw
a
ab
m
mb
42 kDa
26 kDa
17 kDa
10 kDa
4.6 kDa

Figure 8

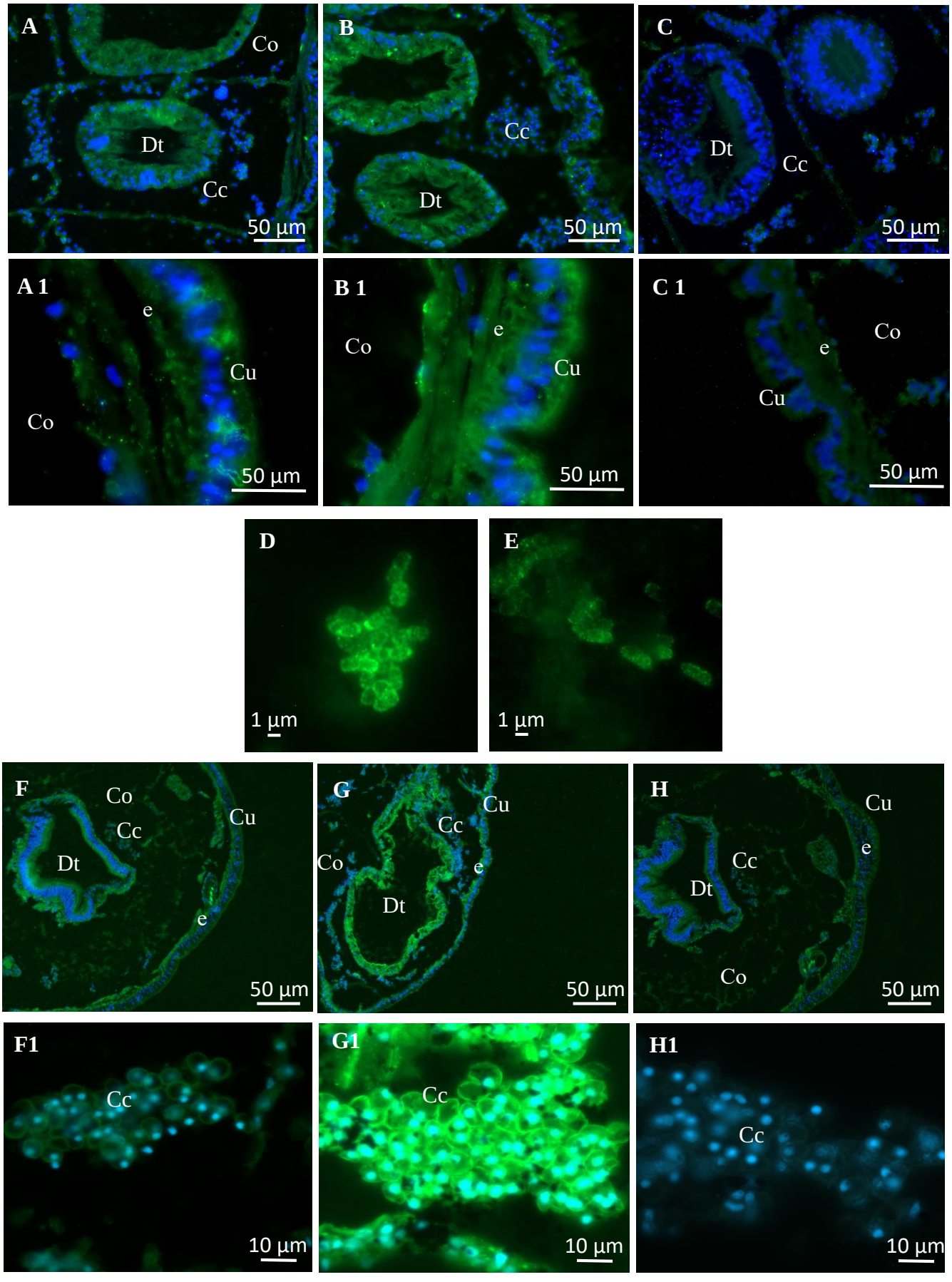
A
Co
Dt
Cc
50 µm
B
Cc
Dt
50 µm
C
Dt
Cc
50 µm
A 1
e
Cu
Co
50 µm
B 1
Co
e
Cu
50 µm
C 1
Co
e
Cu
50 µm
D
1 µm
E
1 µm
F
Co
Cc
Cu
Dt
e
50 µm
G
Cu
Cc
Co
e
Dt
50 µm
H
Cu
e
Cc
Dt
Co
50 µm
F1
Cc
10 µm
G1
Cc
10 µm
H1
Cc
10 µm